

UNCLASSIFIED

AD-A277 059



AR-008-137



DEPARTMENT OF DEFENCE

**DSTO**

**Information Technology Division**

**DTIC**  
SELECTED  
MAR 21 1994  
**S E D**

RESEARCH REPORT  
ERL-0694-RR

SOME DEFENCE APPLICATIONS OF CIVILIAN REMOTE  
SENSING SATELLITE IMAGES

by

Vittala K. Shettigara, Gordon M. Sumerling and Paul J. Whitbread

94-08742



APPROVED FOR PUBLIC RELEASE

UNCLASSIFIED

DTIC

**ELECTRONICS RESEARCH LABORATORY**

**94 3 18 014**

# DISCLAIMER NOTICE



THIS DOCUMENT IS BEST QUALITY AVAILABLE. THE COPY FURNISHED TO DTIC CONTAINED A SIGNIFICANT NUMBER OF COLOR PAGES WHICH DO NOT REPRODUCE LEGIBLY ON BLACK AND WHITE MICROFICHE.

UNCLASSIFIED

AR-008-137



ELECTRONICS RESEARCH LABORATORY

# Information Technology Division

RESEARCH REPORT  
ERL-0694-RR

SOME DEFENCE APPLICATIONS OF CIVILIAN REMOTE  
SENSING SATELLITE IMAGES

by

Vittala K. Shettigara, Gordon M. Sumerling and Paul j. Whitbread

### SUMMARY

This report is on a pilot study to demonstrate some of the capabilities of remote sensing in intelligence gathering. A wide variety of issues, both quantitative and qualitative, are addressed. SPOT satellite images were used for object classification using statistical and neural net techniques, object height determination and image resolution enhancement. A new procedure was developed for detecting small and man-made objects in multispectral or colour images. The procedure will be presented in a separate report.

© COMMONWEALTH OF AUSTRALIA 1993

NOV 93

COPY No.

APPROVED FOR PUBLIC RELEASE

POSTAL ADDRESS: Director, Electronics Research Laboratory, PO Box 1500, Salisbury, South Australia, 5108.

ERL-0694-RR

UNCLASSIFIED

Accession For	
NTIS CRA&I	<input checked="" type="checkbox"/>
DTIC TAB	<input checked="" type="checkbox"/>
Unannounced	<input type="checkbox"/>
Justification	
By	
Distribution/	
Availability Codes	
Dist	Avail and/or Special
A-1	

*This work is Copyright. Apart from any fair dealing for the purpose of study, research, criticism or review, as permitted under the Copyright Act 1968, no part may be reproduced by any process without written permission. Copyright is the responsibility of the Director Publishing and Marketing, AGPS. Inquiries should be directed to the Manager, AGPS Press, Australian Government Publishing Service, GPO Box 84, Canberra ACT 2601.*

---

 CONTENTS

	Page No
ABBREVIATIONS .....	vii
1 INTRODUCTION AND OBJECTIVES .....	1
2 ROLE OF REMOTE SENSING IN DEFENCE .....	2
3 THE STUDY AREA AND THE DATA BASE .....	3
3.1 The study area .....	3
3.2 The data base.....	3
4 PATTERN RECOGNITION.....	13
4.1 Pattern recognition - a brief review .....	13
4.2 Statistical pattern recognition - which technique to use ?.....	14
4.3 Digital Pattern recognition versus aerial photo-interpretation.....	14
4.4 Robustness of common classifiers.....	14
4.5 Choice of classes and training areas .....	16
4.6 Classifications using Maximum Likelihood.....	19
4.6.1 Classification accuracy .....	19
4.6.2 Classification blunders.....	20
4.7 Classifications using Multi-Layer Perceptron .....	27
4.7.1 Some notes on the application of MLPs to classification.....	27
4.7.2 Classification Accuracy.....	31
4.8 Conclusions.....	32
5 OBJECT HEIGHT DETERMINATION.....	33
5.1 Shadow - an important part of images.....	33
5.2 Sun - satellite geometry and the equations.....	33
5.3 Relationship between shadow width, pixel size and intensities .....	36
5.3.1 The role of pixel dimension.....	36
5.4 Shadow Segmentation.....	37
5.4.1 Choosing the threshold for delineating shadow zones.....	37
5.4.2 Measurement of shadow width.....	38
5.5 Result and discussion .....	43
5.6 Some limitations of the technique.....	49
6 NEW IMAGE ENHANCEMENT TOOLS.....	50
6.1 Smooth image zooming .....	50
6.2 Multispectral image enhancement by merging higher resolution panchromatic data.....	54
7 CONCLUSIONS .....	57
BIBLIOGRAPHY.....	59

FIGURES

3.1 Scanned colour aerial photograph of the study areataken on 5 Jan 1987. .... 5

3.2 Multispectral SPOT image of the areataken on 21 April 1987. Pixel resolution 20 m ..... 7

3.3 Panchromatic SPOT image of the area taken on 21 April 1987. Pixel resolution 10 m ..... 9

3.4 Digital map of the area (source AUSLIG). Resolution 1m approximate. .... 11

4.1 Mean spectral responses for 11 super classes with the standard deviations marked ..... 19

4.2 An illustration of the effect of mixing of two classes - light bitumen surface, such as runways, and open fields, such as crop and pastures. .... 21

4.3 Detailed spectral profile of metallic surface and concrete theme classes ..... 24

4.4 Result of maximum likelihood classification after sub-dividing dull metal class. The accuracy figures are with respect to test areas. The overall accuracy of artificial objects is 87.3% ..... 25

4.5 Results of ANN classification using classes selected for GMLC classifier..... 29

5.1 End view of the sun-satellite configuration as seen during imaging..... 34

5.2 Plan view of the sun-satellite configuration as seen during imaging..... 35

5.3 Infrared SPOT image of the study area. The rows of trees used in the study are marked and the buildings whose heights are estimated using the tree shadows are shown at the lower right hand corner..... 41

5.4 Shadow zones, shown as polygons, delineated using the thresholding procedure on the infrared and the panchromatic bands..... 43

5.5 Regression lines for different thresholds. Notice that the estimated heights vary systematically for all the sites except for site 5. Th drastic variation for site 5 is attributed to the inclusion of background areas when the threshold is increased from 1.2 to 1.1s. .... 45

5.6 Variation of estimated tree height with threshold. Notice that the estimated heights converge at two extreme thresholds. Also the variation gradient is maximum between 1.2 and 1.1s..... 46

5.7 A sketch of intensity variation across shadow boundaries to demonstrate the variation of separability at various thresholds. The vertical lines 1, 2 and 3 represent the three sharp boundaries between shadow and background. The three curved lines represent the intensity variation as seen by the sensor across the three boundaries. The lines A, B and O represent the three thresholds and their thickness represents the possible noise level. At thresholds A and B the separation of the three curved lines is difficult to achieve, particularly considering the noise. At threshold O the curves stand separated. .... 47

5.8 A three dimensional display of some rows of trees in the DSTO area..... 47

5.9 The plot of estimated and actual building heights of some industrial buildings..... 49

6.1	Smooth zooming by a factor of 4.	
(a)	the original image of 10m resolution .....	52
(b)	degraded image with 40m resolution .....	52
(c)	image in (b) is smooth zoomed by a factor 4 using cubic convolution, .....	52
(d)	image in (b) smooth zoomed by a factor 4 using the interpolation technique of Newsam(1992) .....	52
6.2	Smooth zooming by a factor of 8.	
(a)	the original image of 10m resolution .....	53
(b)	degraded image with 80m resolution .....	53
(c)	image in (b) is smooth zoomed by a factor 8 using cubic convolution, .....	53
(d)	image in (b) smooth zoomed by a factor 8 using the interpolation technique of Newsam(1992) .....	53
6.3	Merging of panchromatic image with the SPOT multispectral image	
(a)	multispectral image .....	55
(b)	enhanced image by merging panchromatic image .....	55
(c)	Notice the 4 aircraft, below the circular compass swing, near the top right hand corner, enhanced in image (b).....	55

### TABLES

3.1	Imaging Parameters.....	4
4.1	Summary of all the initial 51 training areas.....	17
4.2	Results of the preliminary classification. Top table (confusion matrix) shows accuracy in % for the training areas. Bottom table shows the accuracy in % for the test areas.....	22
4.3	Results of the final classification. Top table (confusion matrix) shows an accuracy in % for the training areas. The second table shows the total number of pixels per theme class for the test areas. The third table (confusion matrix) shows the accuracy in % for the test areas.....	23
4.4	The confusion matrix for MLP classification.....	28
4.5	Comparison of percentage of correct classifications by MLP and GMLC.....	31
5.1	Estimated and actual tree heights.....	44
6.1	Ground control points for zooming by a factor X.....	51

### APPENDICES

I.....	63
II.....	65



---

**ABBREVIATIONS**

ANN	Artificial Neural Network
AUSLIG	Australian Surveying and Land Information Group
BDA	Background Discriminant Analysis
CAD	Computer Aided Design software
DSTO	Defence Science and Technology Organisation
FFT	Fast Fourier Transform
GCP	Ground Control Points
GIS	Geographic Information System
GMH	General Motors Holden
GMLC	Gaussian Maximum Likelihood Classifier
ISI	Image Station Imager - image processing system on Intergraph workstations
LDC	Linear Discriminant Classifier
MLP	Multi-Layer Perceptron, a particular type of ANN
MSS LANDSAT	multi-spectral scanner - Landsat; 80-meter resolution
P SPOT	panchromatic sensor - SPOT; 10-meter resolution
SAR	Synthetic Aperture Radar
SPOT	Systeme Probatoire de l'Observation de la Terre satellite
TM LANDSAT	thematic mapper - Landsat; 30-meter resolution
XS SPOT	Multispectral sensor - SPOT; 20-meter resolution



---

## 1 INTRODUCTION AND OBJECTIVES

Surveillance and intelligence collection have been given the highest priority, particularly at a time of reduced likelihood of hostility (White Paper ,1987). Traditionally the intelligence organisations have heavily relied on high resolution images, mostly from restricted sources. Most of the high resolution images are black and white images, taken in a wide spectral band. Processing of high resolution images is very time-intensive and expensive. The ground resolution of commercial images are coarser than that of the military satellite images. However, this disadvantage can be often offset by the availability of data in more than one spectral band and for a wider area. It is important to weigh the pros-cons of using any type of image data .

In the past, since the launching of the first commercial imaging satellite 21 years ago, the importance of commercial images in surveillance has been greatly ignored. Most of the capability studies in the past (Joye,1991; Richelson,1990) have concluded that the applications of commercial satellite images in surveillance are very limited. Table I.1 in Appendix I summarises this pessimistic view.

However, towards the latter part of 1980s many independent investigators found SPOT pictures very useful in investigating military targets. In order to find out what can be seen from commercial satellites in space , the Carnegie Endowment initiated a series of studies in which SPOT and Soyuzkarta KFA-1000 images were analysed by the professionals in the field. Their results were quite surprisingly different from the earlier pessimistic results. Table I.2 in Appendix I summarises their results (Zimmerman, 1990). The Carnegie Endowment study revealed that what images reveal very much depends on the expertise of the analyser. As such, the processing of the images is a crucial step in deciding whether a set of images is useful or not.

In addition, during the 1991 Gulf war both Landsat and SPOT images were extensively and effectively used (Shettigara V.K.,1992). These aspects prompted us to have a fresh look at the capabilities of commercial satellite images. A comprehensive discussion on the potential of commercial satellite images in wide area surveillance is available in Gale (1992). In this report we present both quantitative and qualitative image processing results to demonstrate that the commercial satellite images are capable of providing much more information than previously believed.

The task ' Intelligence and commercial satellite images ' was a pilot study to evaluate and demonstrate some of the capabilities of commercial satellite images for intelligence gathering purposes. The task was to investigate the capabilities and limitations of the commercially available multi-sensor and multi-band images in detecting and identifying civilian and engineering objects. The task was expected to provide the basis for comparing the performances of some of the traditional and alternate sources of intelligence and mapping in the future.

As listed in the contents, the images were used for feature extraction using statistical and neural net techniques, tree height determination and image resolution enhancement. A separate report is available on a new procedure to detect man-made and small objects in multispectral colour images.

## 2 ROLE OF REMOTE SENSING IN DEFENCE

The term 'Remote Sensing' is used in this report to indicate the study of images from civilian satellites. No regular use is made of remote sensing data in defence, particularly in Australia, for the following reasons: 1. From the defence point view the civilian satellites lack the spatial resolution of military satellites. The best resolution available is 10m. in SPOT digital images and 15 m in synthetic aperture radar images from Almaz satellite. A resolution of 5-7 m is claimed for scanned images produced from the Russian KFA1000 camera. 2. The control of data rests in outside civilian agencies and its availability may not be relied upon at the time of need 3. the revisit time is too far apart for effective reconnaissance and surveillance efforts.

It is reasonable to accept that at present commercial satellite images do not meet some defence needs, particularly at the high resolution end. However, it is reported recently (EOM,1992) that Russian digital images with a resolution of 2-3 m are now available in the open market. As such there is no single source of imagery that could satisfy all the needs of defence. Many issues in, for example, terrain intelligence collection require neither very high resolution nor frequent revisit. To detect activities such as road construction, site clearance for building construction and runway construction the remote sensing data are adequate and probably better because of the multispectral nature. Another major application of remote sensing is in change detection facilitated by the availability of multiple data sources with a good frequency of coverage. The moderate spatial resolution of civilian satellites are advantageous in some terrain analysis applications due to the wide area that a single image can cover. The processing time increases as the inverse square of resolution. It will be wasteful to use higher resolution data when the problem can be solved with lower resolution images. Another attraction of remote sensing is the multispectral character of the data providing spectral resolution in addition to the spatial resolution. The disadvantages of lower spatial resolution can be offset to some extent by the higher spectral resolution. Finally the availability of ever improving, sophisticated but cheap data processing capabilities in micro computers and work stations make the remote sensing technology very attractive.

The 1991 Gulf war clearly demonstrated the role of remote sensing, in conjunction with other sources of information, at both the tactical and the strategic levels. SPOT and Landsat-TM images were extensively used for three major purposes during the Gulf war: 1. to prepare up to date maps of the area, 2. as input to 'automated mission planning systems' (Bernard,1991). and 3. for strategic reconnaissance, particularly using SPOT images. The Gulf war narrowed the technological gap between the military and the civilian technology. (Anson and Cummings, 1991). The work presented in this report will further illustrate the capabilities that are relevant to defence.

### 3 THE STUDY AREA AND THE DATA BASE

#### 3.1 The study area

The Defence Science and Technology Organisation (DSTO) area in Salisbury, about 23 km north of Adelaide, was selected for the study. The site is located around 138°37' E 34°43' S. The area was chosen for the following reasons:

1. Two sets of SPOT satellite images, an airborne SAR image and digital map data were available for the area.
2. The area has a mixture of defence infrastructures, an industrial complex and civilian suburbs. The study area is mainly the DSTO premises and Edinburgh RAAF base, surrounded by the residential suburbs of Salisbury and Elizabeth, and GMH Holden industrial estate. The area has an extensive network of roads of various kinds, railway tracks, and numerous buildings of different types and dimensions. Construction activities are fairly frequent in the area.
3. The northern half of the area is bound by open fields and farm lands.
4. One of the important requirements of remote sensing studies is the need to collect ground truth data. From this point of view the area was readily accessible for research purposes.

The terrain is flat. The eastern portion of the area has been planted with rows of trees that run roughly north-east and north-west. The rows consist of either aleppo pines or sugar gums. At places both types of rows are seen side by side, with usually the aleppo pine rows in the south and the sugar gum rows in the north. The rows of trees surround open fields and factory like buildings. Most buildings have asbestos saw-tooth roof with south lighting. A few have tin roofs.

The Edinburgh Air base on the north western part of the area has a sealed runway in the N-S direction, taxi ways and apron areas for aircraft parking. There is a disused unsealed runway in the NE direction. The major buildings are near the hangars adjoining the apron, to the east of the main runway. The administrative buildings of the air base and the residential quarters are situated to the east of the airfield. An ammunition storage facility exists near the runway.

#### 3.2 The data base

One multispectral and two SPOT panchromatic images were utilised in this study along with two aerial photographs. No image processing has been done on the photographs as they were used only for reference. The first panchromatic image and the multispectral image were taken on 21st April 1987 where as the second panchromatic image was taken on 25 April 1987. The panchromatic images are off nadir looking and form a stereo pair. The image parameters are summarised in Table 3.1.

The first aerial photograph was taken on 5th January 1987 and the second was taken on 3rd October 1990. The scanned aerial photo of 5th January is shown in Figure 3.1, with a pixel resolution of 1.6 m. This aerial photograph was taken 109 days before the satellite images were acquired. The terrain conditions as seen in the photograph, particularly with regard to vegetation, may not be the ambient condition when the satellite images were collected.

The Panchromatic image of the 25th April (not shown) and the Multispectral image (Figure 3.2) of the 21st April were registered on to the Panchromatic image of the 21st April (Figure 3.3) utilising nearest neighbour sampling and first order polynomial transformation. This involved resampling the Multispectral image from twenty metre pixels to ten metre pixels. All the processing was done on this set of images.

Table 3.1 Imaging Parameters

Satellite:	SPOT 1	SPOT 1
Date:	21/4/87	25/4/87
Local Time	10. 06. 05.	10. 29. 18.
Latitude:	S 34° 53' 39"	S 34° 53' 39"
Longitude:	E 138° 33' 32"	E 138° 35' 13"
Orientation:	12.9°	9.2°
Incidence:	R 23.4°	L15.5°
Azimuth:	39.2°	32.1°
Elevation	34.5°	36.2°

In Figure 3.4 is a part of the existing GIS vector data base imported from the Australian Surveying and Land Information Group (AUSLIG). The accuracy of the data is about 1 m. This vector based data can be overlain on the raster images and information extracted from the images can be added to the vector data base. The information collected and stored in the vector data base can annotated and displayed with ease.

The data processing in this task was done on an Intergraph workstation using ISI-2 image processing software and locally developed computer programs.

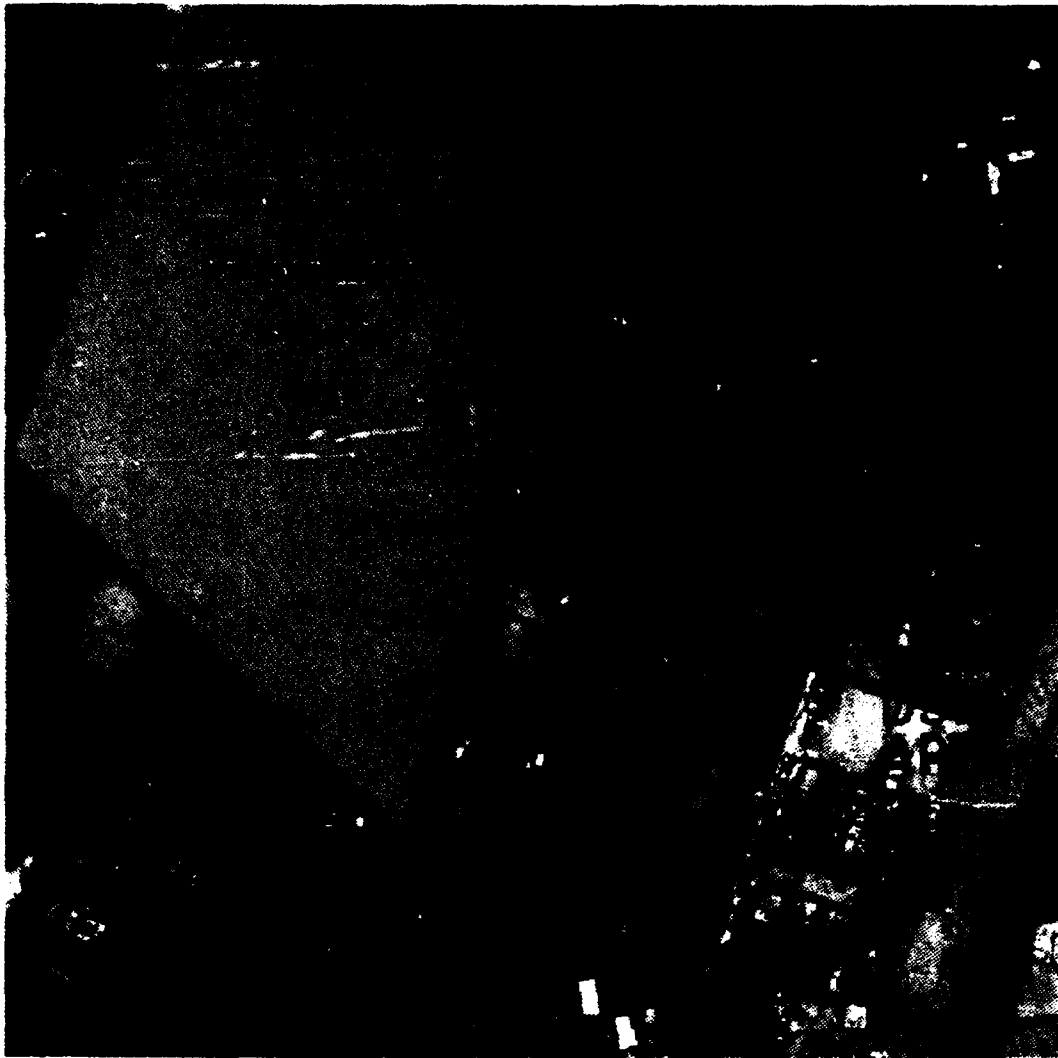


Figure 3.1 Scanned colour aerial photograph of the study areataken on 5 Jan 1987.

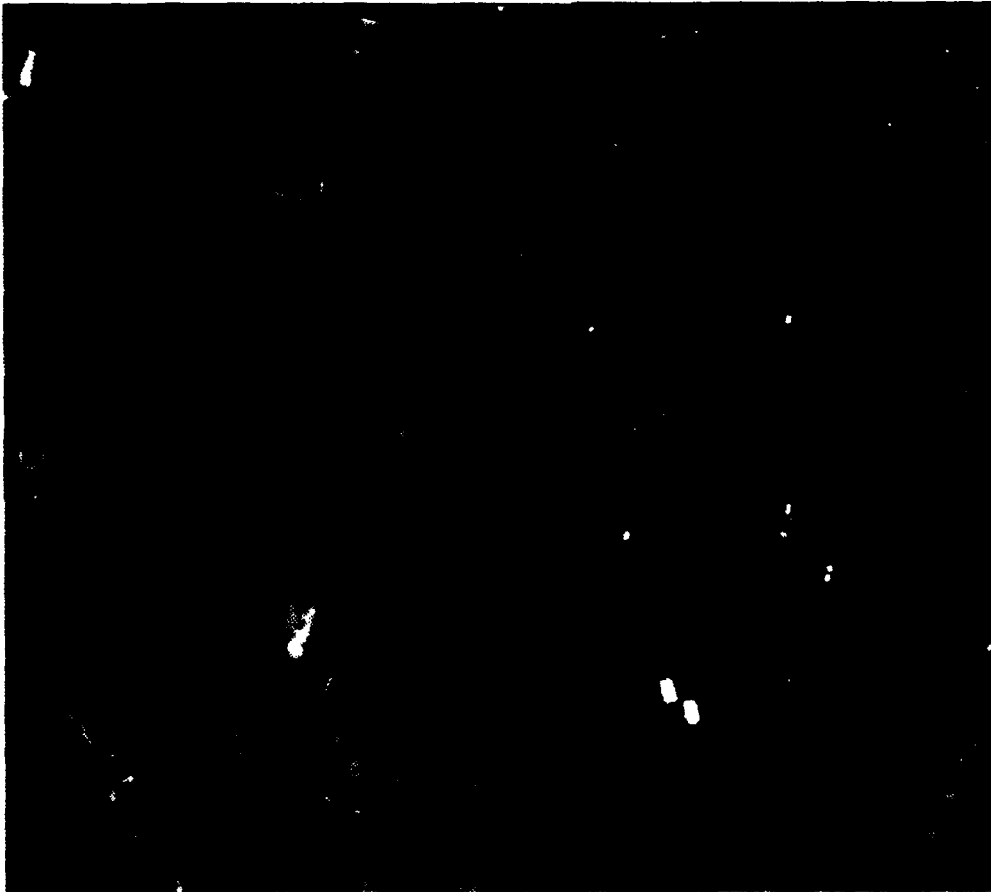


Figure 3.2 Multispectral SPOT image of the areataken on 21 April 1987. Pixel resolution 20 m



Figure 3.3 Pancromatic SPOT image of the areataken on 21 April 1987. Pixel resolution 10 m

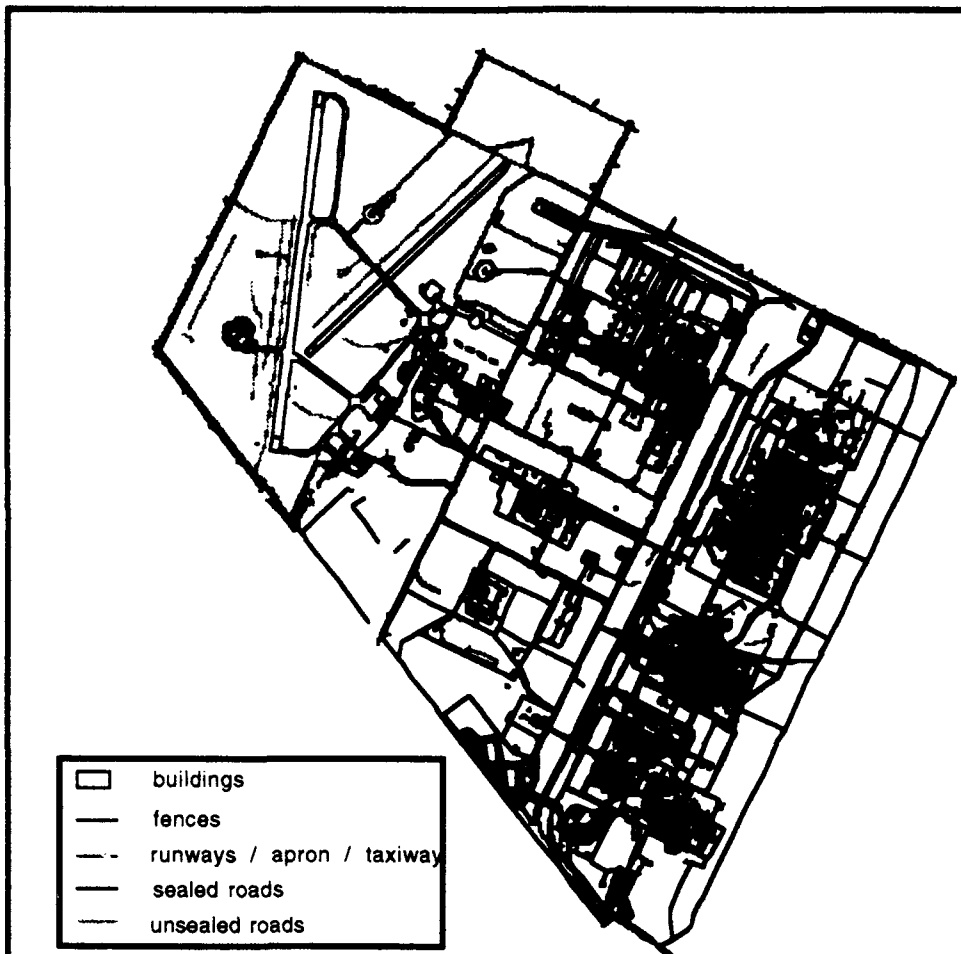


Figure 3.4 Digital map of the area (source AUSLIG). Resolution 1m approximate.

---

## 4 PATTERN RECOGNITION

The term pattern recognition is used to mean various aspects in image processing literature. Pattern recognition is a classification problem, including clustering and supervised classification (Young and Calvert, 1974). Prior to classification, however, a detection stage may be involved depending on the technique used. Sometimes the term 'pattern recognition' is stretched to include image enhancement. Some authors constrain it to mean 'image understanding' that is mainly concerned with representing real world objects and managing them in a computational environment (Sleigh, 1983). Feature extraction is another term frequently used to mean pattern recognition. However, the use of the term 'feature extraction' will be avoided in this report as the term 'feature' is some times used to mean the bands in the image and feature extraction in such a context refers to the selection of features (bands) or the reduction of the dimensionality of the data set without significantly losing the information content. In this report, 'Pattern recognition' is used to mean the classification of the images to objects of known physical description.

### 4.1 Pattern recognition - a brief review

There are three main approaches to pattern recognition:

- (a) statistical pattern recognition,
- (b) optical and digital pattern correlation (template matching), and
- (c) model-based vision. A good review of these techniques is available in Mundy (1991).

Statistical pattern recognition can be implemented using Bayesian classifiers, clustering procedures or more recently neural-net classifiers. The strength of statistical pattern recognition lies in its ability to process multi-dimensional data in a multi-dimensional space without knowing the spatial structure of the data. However, with some difficulty the spatial structure of the data may be incorporated in the statistical procedures for a better result. Other techniques described below process variates of the multivariate data separately.

In the technique of pattern correlation, an instance of the object is taken as a template and its correlation with different parts of the input image is determined. The targets are determined based on maximum correlation achieved. Correlation techniques can be made translation, rotation and scale invariant. However, correlation is not intensity invariant. Variation in shadows can give false results (Mundy, 1991).

In model based pattern recognition procedures the image is initially processed to extract a 2D description of the objects. Then, using a 3D model, a 2D representation is predicted. The classification is achieved based on the prediction accuracy. The advantage of this technique is that it is intensity invariant. However, the technique suffers as the pixel resolution becomes coarser. This limits its application in pattern recognition in civilian satellite images.

From the above discussion it is clear why the statistical pattern recognition is still the favoured approach in remote sensing applications.

#### **4.2 Statistical pattern recognition - which technique to use ?**

In the image classification context two terms are commonly encountered: feature class and information class. Feature classes refer to data clusters having similar statistical properties and they may or may not have any bearing on objects that we recognise. On the other hand information classes refer to classes of objects that we identify as types of land cover.

The discrimination processes used for extracting feature classes are commonly called 'clustering'. Clustering is mainly used for studying the data structures in terms of separable groups of data points. As this process requires no supervision whilst training the process to identify objects it is called 'unsupervised classification'. This process is not generally used in remote sensing investigations as the clusters are hard to relate to the terrain objects that the user intends to investigate.

Information classes are extracted from the images by training a statistical process to recognise objects from their spectral properties. The processes are trained to discriminate between information classes by providing a sufficiently large number of samples, usually more than 100, of each information class. As the user supervises the process during training, the technique is called 'supervised classification'. In this report only supervised classification techniques are used.

#### **4.3 Digital Pattern recognition versus aerial photo-interpretation**

Digital classification of satellite images can produce a greater variation within information classes than visual interpretation of aerial photographs or ground truthing can produce, particularly regions of uniform texture (Sali and Wolfson, 1991, Hyland *et al*, 1988). This issue is explained in Klemas *et al* (1975) with examples. The finer resolving power of the classifiers can often be disadvantageous as it causes graininess or 'salt and pepper effect' in classification results.

To overcome the graininess of the classification a post-classification, line preserving smoothing filter was passed over many of the classified images in this report. The filter is a part of the ISI-2 image processing software. The effect of this is to remove any single or isolated small groups of pixels that represent the finer classification not perceived by the human eye. It does however preserve groups of pixels of a prescribed length or greater that could represent linear features in the classified image. All GMLC classified results shown in this report are post-processed.

#### **4.4 Robustness of common classifiers**

In developing classification procedures one may encounter following three possibilities (Lachenbruch and Goldstein, 1979):

1. the probability distribution of data is completely known,

2. the probability distribution of data is known or assumed but the parameters are unknown,
3. nothing whatever is known and a distribution is not assumed

In remote sensing applications the first case is very rare. If the distribution is completely known the posterior probability may be easily computed and the pixel can be assigned to the class with the highest probability. The second case is very common and usually a multivariate normal distribution is assumed. The unknown parameters are obtained from the maximum likelihood estimates of training areas. Class membership is assigned according to the maximum likelihood rule.

In the second case, nothing is assumed about the underlying multivariate distribution and the procedures are called non-parametric; that is, they are distribution free. In principle non-parametric procedures should provide better results if the samples are large, as in remote sensing applications, and when the distributions are not normal (Lachenbruch and Goldstein,1979).

Two classifiers are well known in classification or discriminant analysis literature: Fisher's linear discriminant classifier (LDC) and Gaussian maximum likelihood classifier (GMLC). Both of these techniques provide optimal results when the data have a Gaussian or Normal distribution.

GMLC is by far the most widely used classifier in remote sensing studies. By definition, the classifier assumes multivariate normal distribution for data points. Although this assumption is violated by most of the data set we encounter, the technique works very well. The technique is fairly robust to violation of Gaussian model (Richards,1986).

LDC is not commonly used in remote sensing investigations. However it has certain qualities, apart from the simplicity of its implementation, which merit brief consideration here. Shettigara (1991a) has compared the performance of LDC and GMLC. His study showed that LDC is more robust than GMLC. LDC is widely and quite erroneously associated with multivariate distribution. It is true that LDC gives optimal results for multivariate normal data. However, it is not restricted to any particular distribution. The technique maximises distance, in spectral data space, between class means (Anderson,1982). LDC is a legitimate non-parametric technique.

Another family of non-parametric techniques that have become popular recently is based on Artificial Neural Networks (ANNs). A particular kind of ANN, the multi-layer perceptron (MLP) can be used for supervised classification. The MLP does not use any data distribution model and in principle should be able to fit the best possible decision surface between two classes, giving 100% accuracy for separable classes. In practice such accuracy is not achieved for a variety of reasons; e.g. training is a long process and is often curtailed. Some researchers claim that ANNs perform better if they are trained on properly pre-processed data sets (Iisaka and Russell,1991). However, most cases documented in the literature do not share this view. In general, accuracy has been found to be comparable with standard GMLC techniques (Benediktsson and Swain, 1990; Hepner *et al.*, 1990; Sheldon, 1990; Kanellopoulous *et al.*,

1991; Heermann and Khazenie, 1992). The results of using ANNs for classification are presented later in the section.

#### 4.5 Choice of classes and training areas

To classify an image using supervised classification, areas need to be selected that are representative of classes chosen. These areas, known as training areas, are the key to a successful classification. When selecting training areas for supervised classification three important factors should be considered (Ioka and Koda, 1986). The training areas should

- (a) fully reflect categorised theme information which is visually interpreted and recognised,
- (b) contain all possible multispectral features inherent in each category, and
- (c) satisfy the *a priori* statistical assumptions/conditions of the classification procedures.

As stated, training data have to represent as much spectral variation within the class as possible. This is particularly highlighted by Wright and Harris (1988). They found that the accuracy of classification improved when more than one training area represented a class. In this study, initially 51 known training areas were chosen using the knowledge gained from analysing aerial photographs and extensive ground truthing of the study area. All the 51 training areas are identified in a theme file by giving a unique number to pixels in each training area (Table 4.1). All the training areas represent a recognisable land cover (class) and care was taken not to overlap boundaries into other classes.

The 51 training areas were then reduced to 11 super-training areas (classes) initially, by merging training sets as shown in Table 4.1. Later, one of the classes, dull metal, was further divided into two classes, namely dull metal and specular metal. The reason for this will be explained later in this section. The merging of training areas was necessary because many training areas represented a single meaningful physical class.

To decide how to merge smaller training sets into super-training sets, graphical and statistical techniques were used apart from considering the physical appearance. The multispectral data for each training area were plotted as scattergrams and their distributions relative to other classes were used as a guide to pool some of the training areas. The Jeffries-Matusita (J-M) distance measure was also used as a guide to merge different training areas. J-M distance is a statistical measure for determining the separability of 2 classes. As the separability increases, the J-M distance asymptotically approaches a value of 2.0. The distance measure has the advantage of varying the measure scale by stretching the smaller class separations and contracting larger class separations.

Table 4.1 Summary of all the initial 51 training areas

Class name	description	Theme	No of pixels
Sugar Gums	Aerodynamics area	11	104
	Aerodynamics area	12	126
	Aerodynamics area	13	96
	Boundary Aerodynamics and RAAF	14	120
	East contactors area	15	129
Aleppo Pines	NW of army logistics base	21	84
	NW of army logistics base	22	84
	Between DSTO and RAAF along disused railway line	23	54
	2 km south of above site	24	47
Open fields and Grassland	250 m NW of Angle Vale Rd and rail crossing	30	1374
	150 m E of Angle Vale Rd and rail crossing	31	1692
	Between dirt and bitumen runway	32	240
	1000 m south of old train circle	33	143
	500 m east of near civil construction	34	266
	100 m west of Elizabeth South train station	35	395
	North field of DSTO area	36	987
	200 m south of runway	37	967
	Between Labs and Contractors area	38	535
Top NW corner of the image	39	520	
Lawns	RAAF oval - north	41	108
	RAAF oval - south	42	96
	DSTO north golf oval	43	72
	Elizabeth Oval	44	156
Dull metallic surface	Metallic hanger-RAAF base	52	21
	87 labs	53	15
	Maintenance and workshops	54	37

<b>Bright Metallic Surface</b>		
stores north building	61	83
<b>Asbestos Surface</b>		
77 Labs	71	36
40 Labs (library)	72	16
102 Contactors	73	39
275 Aerodynamics area	74	16
71 Labs	75	32
<b>Dark Apron - Edinburgh airbase</b>		
west compass swing	81	40
south compass swing	82	54
east compass swing	83	36
visiting aircraft apron	84	63
<b>Light Apron - Edinburgh airbase</b>		
North of hangers	91	90
North of hangers	92	21
Between hangers	93	56
North of hangers	94	33
South end of runway	95	185
North end of runway	96	237
<b>Specular Metallic Surface</b>		
GMH	101	591
dull hanger - Edinburgh airbase	102	20
<b>Concrete Surface - Edinburgh airbase</b>		
compass swing	111	38
engine test bay	112	47
North piano keys	113	28
<b>Barren Soil Surface</b>		
east of horse track and 500 m		
west of runway	121	57
south of horse track and 500 m		
west of runway	122	89
Road 150 m south of runway	123	64
horse track 500 m west of runway	124	68

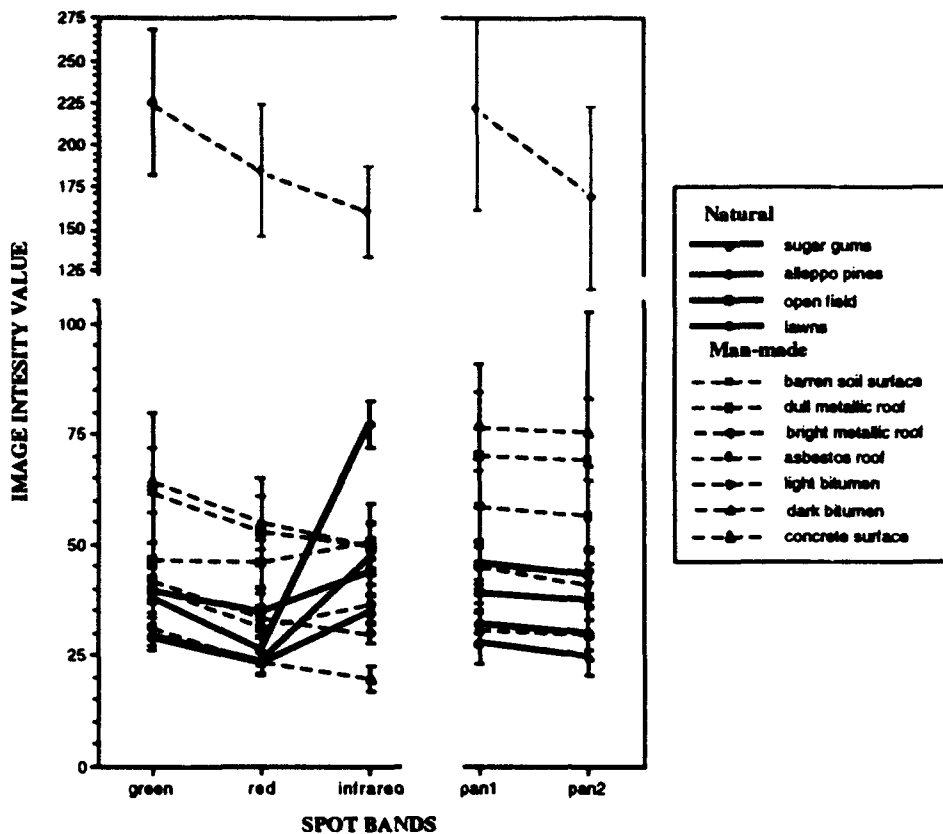


Figure 4.1 Mean spectral responses for 11 super classes with the standard deviations marked

## 4.6 Classifications using Maximum Likelihood

### 4.6.1 Classification accuracy

The confusion matrix in Table 4.2 shows the initial classification results from using GMLC. The overall accuracy of the classification in the test areas is 82% that is not entirely satisfactory. It is felt that an error of about 10% is tolerable, in a subjective sense. Most errors are in three classes: open fields, dull metallic roof and dark bitumen. The misclassification is particularly predominant amongst artificial objects. However, very few natural objects are misclassified as artificial objects, indicating that the commonly occurring artificial objects are quite distinguishable from natural objects in spectral domain.

The misclassification in open fields is due mainly to the inhomogeneity in the class. This can be seen from the individual training areas within the class, as shown in Table 4.1. The class might have included, as a part of the open fields, some sparsely vegetated soil covers which are classified as barren soil covers. As no aerial

photographs contemporaneous with the SPOT images are available, it is difficult to ascertain if the confused areas were low in vegetation.

The confusion matrix reveals few other interesting properties. Amongst artificial objects most of the misclassification occurs between objects of similar nature. For example, a significant amount of pixels in dull metallic roof is classified as bright metallic roof. Similarly quite a big number of dark bitumen pixels is misclassified as light bitumen. This misclassification can be generally tolerated as they represent similar materials and their differentiation may not be necessary for most of the applications.

#### 4.6.2 Classification blunders

The confusion matrix does not reflect the true cost of classification or mis-classification. In some cases, although the percentage error in misclassification is small, from the defence point of view the misclassification can be considered serious. Such errors are grouped as blunders. Blunder detection should become an important part of any classifier.

For GMLC, there are a couple of misclassifications of serious nature. 12.8% of dark bitumen pixels are misclassified as bright metallic surfaces. Spectrally these two classes are quite different as shown in Figure 4.1. The metallic surfaces are highly reflective in all the bands while the dark apron is highly absorptive in all bands. The J-M distance between the classes is 1.99, which indicates that the two classes are quite separable. This suggests that the misclassification is not due to the overlapping of classes. A closer examination of the dark bitumen test area revealed that there were aircraft parked on the bitumen that were barely visible in the original multispectral image. The features in the test area are in fact stationary aircraft on the bitumen. Aircraft are metallic and so show a similar spectral response to the metallic class. As such, the pixels have been correctly classified as metallic surface on the dark bitumen surface. This demonstrates the capability of a simple classifier to detect small objects of distinct spectral signature in relation to their background. The object may not be visible due to their small size in relation to the pixel size and/or due to mixing of two or more signatures.

Another serious misclassification has occurred in light bitumen class. 3% for the bitumen area (Table 4.2), which may be normally considered insignificant, has been misclassified as asbestos. These errors occur along the boundary between the open field and light bitumen classes. The reason for this error is suspected to be due to mixing of open field and light bitumen classes. In Figure 4.2 spectral profiles for light bitumen, open fields and asbestos surfaces are shown. A profile for the mixed class with equal parts of open fields and light bitumen classes is presented. As can be seen the spectral profiles, open fields and light bitumen classes are distinct particularly in the infrared band. However, when these two spectral classes are combined in various proportions it is easy to see that the resulting pixel will have a profile similar to that of asbestos

surfaces. This illustrates that it is easy to confuse mixed pixels for a totally different object.

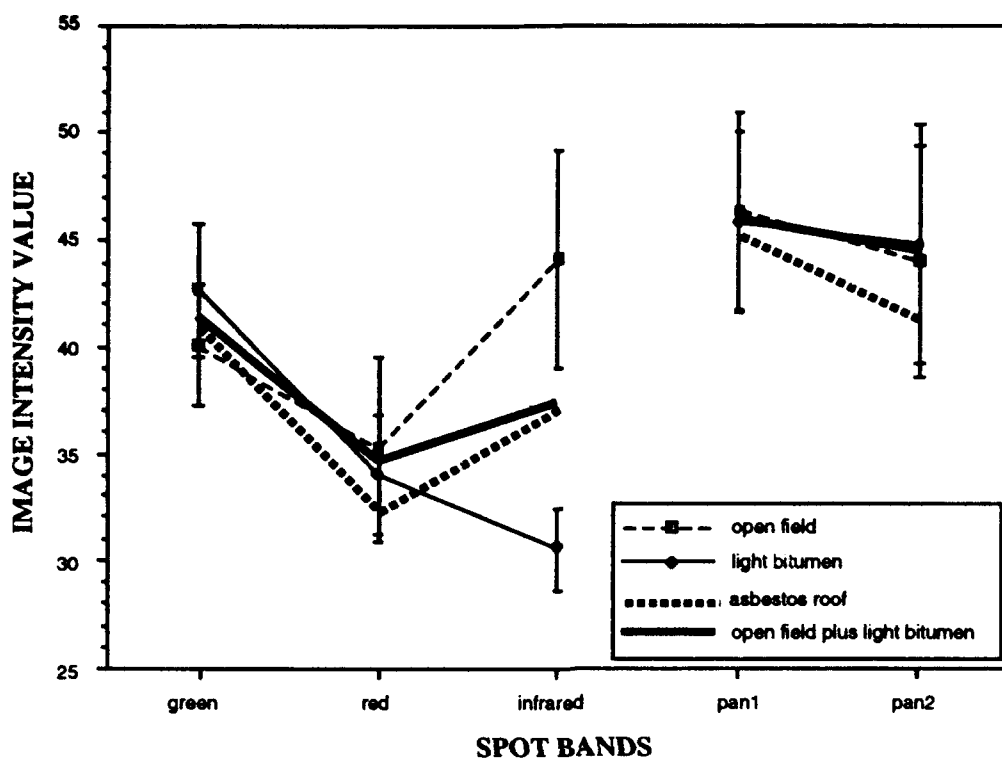


Figure 4.2 An illustration of the effect of mixing of two classes - light bitumen surface, such as runways, and open fields, such as crop and pastures.

Another significant misclassification has occurred between dull metallic surface and concrete surface. A high percentage of dull metallic surface class has been labelled as concrete surface. From Figure 4.3 it can be seen that the spread of the concrete surface training areas is relatively small and as such this class splits the dull metallic class into two distinct classes. This indicated a need for the dull metallic surface theme class to be split into two classes.

	Sugar Gums	Aleppo Pines	Open Fields	Lawns	Gravel Roads	Dull Metallic Roof	Bright Metallic Roof	Asbestos Roofs	Dark Bitumen	Light Bitumen	Concrete	
Sugar Gums	100	0.15	0.15	0.15	0.15	0.15	0.15	0.15	0.15	0.15	0.15	
Aleppo Pines	3.75	100	1.67	1.25	1.25	1.25	1.25	1.25	1.25	1.25	1.25	
Open Fields	1.09	1.09	100	2.51	2.51	2.51	2.51	2.51	2.51	2.51	2.51	
Lawns	1.21	1.21	1.21	100	1.36	1.36	1.36	1.36	1.36	1.36	1.36	
Gravel Roads	1.21	1.21	1.21	1.21	100	59.13	3.17	0.15	0.15	0.15	36.04	
Dull Metallic Roof	1.21	1.21	1.21	1.21	1.21	100	0.61	84.24	6.06	1.82	0.50	
Bright Metallic Roof	1.21	1.21	1.21	1.21	1.21	1.21	100	0.50	7.46	90.05	0.50	
Asbestos Roofs	1.21	1.21	1.21	1.21	1.21	1.21	1.21	100	0.50	0.50	0.50	
Dark Bitumen	1.21	1.21	1.21	1.21	1.21	1.21	1.21	1.21	100	0.50	0.50	
Light Bitumen	1.21	1.21	1.21	1.21	1.21	1.21	1.21	1.21	1.21	100	0.50	
Concrete	1.21	1.21	1.21	1.21	1.21	1.21	1.21	1.21	1.21	1.21	100	
accuracy												87.38

	Sugar Gums	Aleppo Pines	Open Fields	Lawns	Gravel Roads	Dull Metallic Roof	Bright Metallic Roof	Asbestos Roofs	Dark Bitumen	Light Bitumen	Concrete	
Sugar Gums	100	0.80	0.80	0.80	0.80	0.80	0.80	0.80	0.80	0.80	0.80	
Aleppo Pines	7.89	100	3.25	3.25	3.25	3.25	3.25	3.25	3.25	3.25	3.25	
Open Fields	0.62	0.62	100	99.38	99.38	99.38	99.38	99.38	99.38	99.38	99.38	
Lawns	0.62	0.62	0.62	100	53.61	28.87	17.53	17.53	17.53	17.53	17.53	
Gravel Roads	0.62	0.62	0.62	0.62	100	13.33	80.00	4.44	4.44	4.44	4.44	
Dull Metallic Roof	0.62	0.62	0.62	0.62	0.62	100	1.68	3.02	2.35	2.35	2.35	
Bright Metallic Roof	0.62	0.62	0.62	0.62	0.62	0.62	100	0.80	0.80	0.80	0.80	
Asbestos Roofs	0.62	0.62	0.62	0.62	0.62	0.62	0.62	100	0.80	0.80	0.80	
Dark Bitumen	0.62	0.62	0.62	0.62	0.62	0.62	0.62	0.62	100	0.80	0.80	
Light Bitumen	0.62	0.62	0.62	0.62	0.62	0.62	0.62	0.62	0.62	100	0.80	
Concrete	0.62	0.62	0.62	0.62	0.62	0.62	0.62	0.62	0.62	0.62	100	
accuracy												82.018

Table 4.2 Results of the preliminary classification. Top table (confusion matrix) shows accuracy in % for the training areas. Bottom table shows the accuracy in % for the test areas.

	Sugar Cums	Alleppe Pines	Open Fields	Lawns	Barren Soil	Dull Metallic Roof	Specular Metallic Roof	Bright Metallic Roof	Asbestos Roofs	Dark Bitumen	Light Bitumen	Concrete
Sugar Cums	3.75	94.17	1.67						0.42			100.00
Alleppe Pines	1.09			98.91								100.00
Open Fields												100.00
Lawns												100.00
Dirt Roads					1.15	98.40						3.45
Dull Metallic Roof								100.00				100.00
Specular metallic roof												100.00
Bright Metallic Roof												100.00
Asbestos Roofs		0.23	2.80			0.23			4.20	89.28	3.26	100.00
Dark Bitumen												100.00
Light Bitumen					1.53	0.76	6.87					100.00
Concrete												90.84
accuracy												90.89
Sugar Cums	12	135	5									225
Alleppe Pines	2			321								152
Open Fields												677
Lawns												323
Dirt Roads						37						131
Dull Metallic Roof												46
Specular Metallic Roof								116				153
Bright Metallic Roof						4						120
Asbestos Roofs										109		78
Dark Bitumen												109
Light Bitumen							14					298
Concrete												92
accuracy												2406
												84.41
Sugar Cums	7.89	88.82	3.29									100.00
Alleppe Pines	0.62			99.38								100.00
Open Fields												100.00
Lawns												100.00
Dirt Roads												100.00
Dull Metallic Roof						77.08						22.92
Specular Metallic Roof												100.00
Bright Metallic Roof						3.33		96.67				100.00
Asbestos Roofs										100.00		100.00
Dark Bitumen												100.00
Light Bitumen												100.00
Concrete							15.22					84.78
accuracy												84.41

Table 4.3 Results of the final classification. Top table (confusion matrix) shows an accuracy in % for the training areas. The second table shows the total number of pixels per theme class for the test areas. The third table (confusion matrix) shows the accuracy in % for the test areas

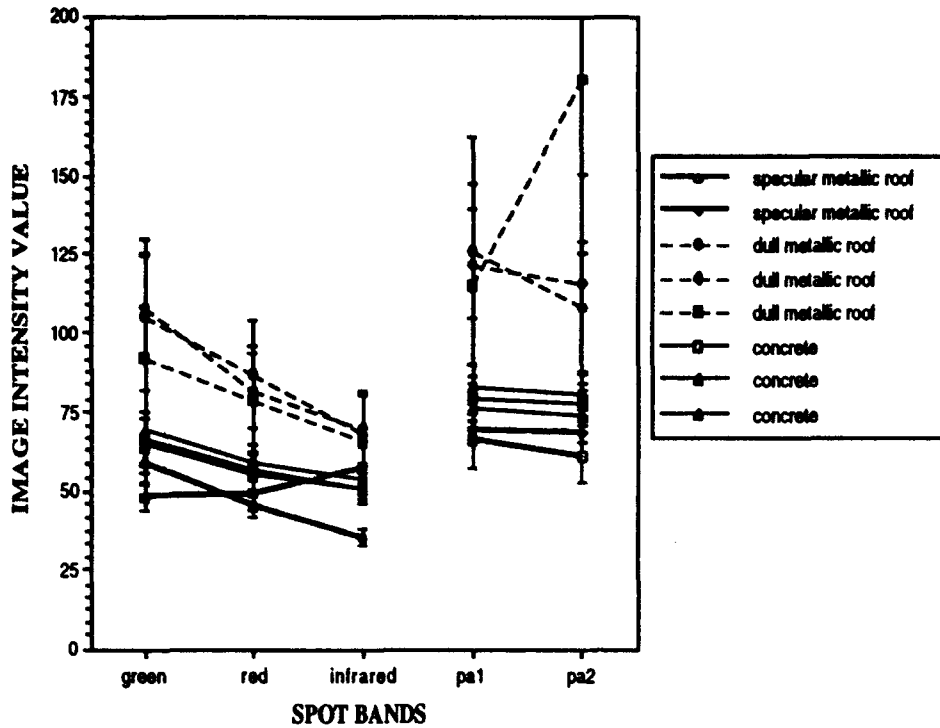


Figure 4.3 Detailed spectral profile of metallic surface and concrete theme classes

The J-M distance between the dull metallic and concrete classes is only 1.2059. Using the relationship between the J-M distance and the probability of error (Swain and Davis,1978) the maximum error in classification is estimated to be of the order of 13.6%, given equal prior probability for the two classes. This indicates that the two classes are fairly separable. However, the actual error observed is very high. One of the possible reasons for this is that the probability distribution function (pdf) assumed for one or both the classes may be wrong. A look at the scattergrams of the dull metallic class revealed that it is bimodal, which seriously violates the assumption that data have normal distribution.

As a result of this finding a further classification was performed, where the dull metallic class was split into two classes, dull metallic and specular metallic surface. Table 4.3 is the confusion matrix for the new classification. Note that the overall accuracy of the image classification has improved from 87.38% in the first classification to 90.49% in the second classification if the accuracy test is done on the training area. However, if the accuracy is computed on a number of test areas the overall accuracy drops slightly, from 82 % to 81.2%. Bulk of the error is in the open field class. If we consider only the artificial objects the overall accuracy has improved from 81.2 % to 87.3 % in the second classification. This level of accuracy is closer to the target accuracy of 90% set in the beginning of the study. The open field class probably needs to be further sub-divided into two or more sub-classes in order to improve the overall accuracy. The new classified image is seen in Figure 4.4



Maximum Likelihood classification

man-made		Accuracy %	natural		Accuracy %
	barren soil surface	98.47		gums	85.78
	dull metallic surface	77.08		pinos	88.82
	specular metallic surface	87.58		open fields and grassland	69.28
	bright metallic surface	96.67		lawn	99.38
	asbestos surface	97.44			
	dark bitumen surface	100			
	light bitumen surface	78.52			
	concrete surface	84.78			

overall classification accuracy 84.41 %

Figure 4.4 Result of maximum likelihood classification after sub-dividing dull metal class. The accuracy figures are with respect to test areas. The overall accuracy of artificial objects is 87.3%

---

## 4.7 Classifications using Multi-Layer Perceptron

### 4.7.1 Some notes on the application of MLPs to classification

The classification power of the multilayer perceptron has been recognised for a number of decades, but only since the work of Rumelhart *et al* (1986) has it been possible to train the MLP from example data. A detailed definition of the MLP and a description of the method of training for this application is given by Whitbread (1992). Since the application of MLPs to classification of remotely sensed data is relatively new technology, some comments on its limitations and difficulties of implementation are included here.

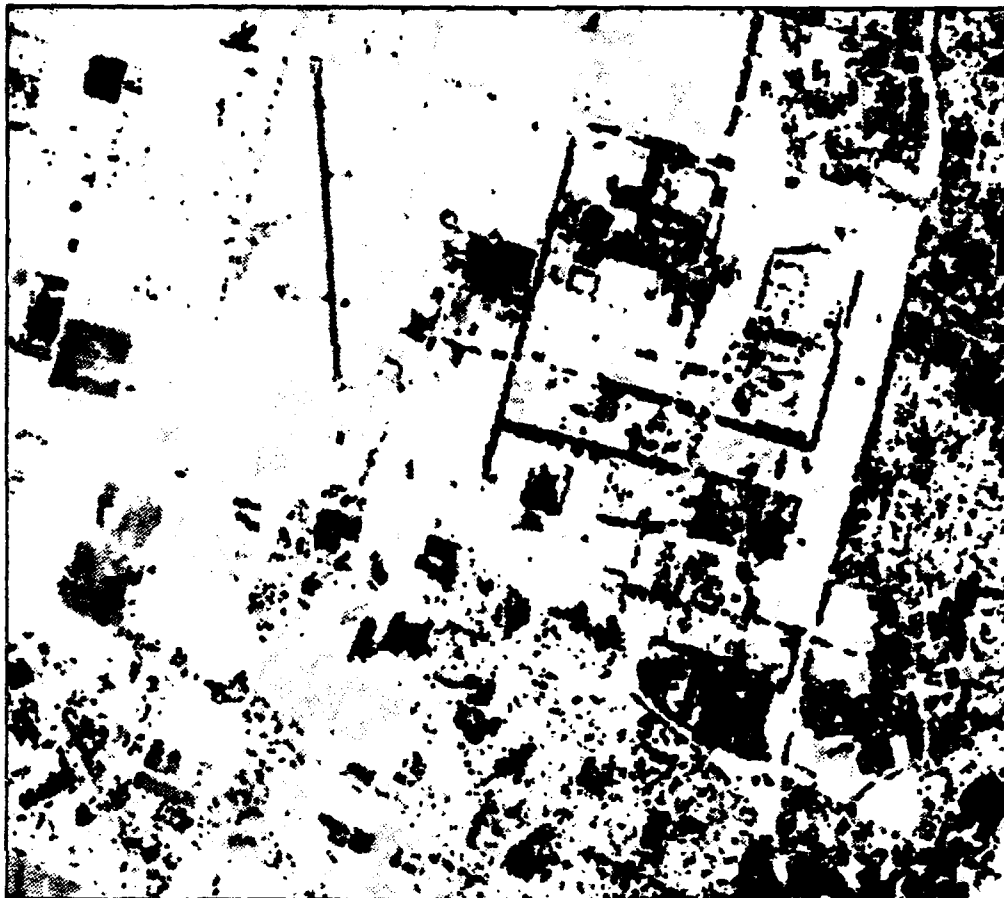
The MLP is attractive as a classifier because it is essentially model free, and during training learns not only the parameters of a class but also the data's probability distributions. In situations where there are naturally occurring non-normal distributions (which challenge GMLC) it is possible to produce an optimal classifier. A particular case of non-normally distributed data is auxiliary data such as digital elevation data, which could improve classification accuracy when combined with remotely sensed data. The MLP is also of interest because of the potential to realise it in hardware as a fast parallel classifier. However, results presented in this report are based solely on simulation.

The MLP has not been embraced by the bulk of users of classification processes because of some limitations in implementation. Firstly, the MLP is slow to learn; whereas the GMLC measures its required parameters by a single inspection of the training data, an MLP learns its parameters by continued re-inspection of the training examples. Commonly 20,000 inspections can be required to achieve 1% accuracy, and currently most MLP classification is done by simulation that multiplies overheads. The second problem is that there is no current theoretically based method for choosing the size of the MLP necessary for a particular classification task, but it is clear that size is important. The current approach is to choose the size using heuristics combined with trial and error. Heuristics for choosing the MLP size for the task of classifying remotely sensed data were developed by Whitbread (1992). The third problem is reliability. Internally, the MLP is a non-linear system, which makes it hard to predict its behaviour as data quality becomes poor. In model based systems (such as GMLC) we expect "graceful degradation" of behaviour.

Despite these limitations, the MLP promises potentially better classification accuracy than conventional classifiers, and as well promises greater ease of use, since it is not necessary to choose training sets that satisfy the *a priori* statistical assumptions of the conventional procedures (see paragraph 4.5 (c) above).

	Sugar Gums	Aleppo Pines	Open Fields	Lawns	Barren Soil	Dull Metallic Roof	Specular Metallic roof	Bright Metallic Roof	Asbestos Roof	Dark Bitumen	Light Bitumen	Concrete
Sugar Gums												100.00
Aleppo Pines	93.42		6.58									100.00
Open Fields												100.00
Lawns	0.62			99.38								100.00
Barren Soil												100.00
Dull Metallic Roof					16.67	5						33.33
Specular Metallic roof												100.00
Bright Metallic Roof								90.00				100.00
Asbestos Roof												100.00
Dark Bitumen									75.23		24.77	100.00
Light Bitumen												100.00
Concrete					8.70		39.13					52.17
												79.31

Table 4.4 The confusion matrix for MLP classification



**Neural Network classification**

<b>man-made</b>		<b>Accuracy %</b>	<b>natural</b>		<b>Accuracy %</b>
	barren soil surface	98.47		gums	73.33
	dull metallic surface	50.00		pinos	93.42
	specular metallic surface	97.39		open fields and grassland	64.84
	bright metallic surface	90.00		lawn	99.38
	asbestos surface	83.33			
	dark bitumen surface	75.23			
	light bitumen surface	74.16			
	concrete surface	52.17			

**overall classification accuracy 78.68 %**

**Figure 4.5 Results of ANN classification using classes selected for GMLC classifier.**

#### 4.7.2 Classification Accuracy

The purpose of the results presented here is to show the utility of the MLP classification method. The results are based on the same training areas as the results from GMLC presented above and they do not take advantage of the possibility of relaxing the requirement paragraph 4.5(c) in the choice of training areas.

The MLP used for classifying the multispectral data had three (active) layers comprising 50, 6 and 12 nodes in the first, second and third layers respectively. The MLP was trained by adjusting its internal weights using the back propagation procedure of Rumelhart, *et al.* (1986). (The learning rate was 0.01 and momentum 0.0.) Training was limited to 20,000 iterations, representing approximately 1600 presentations of examples per class. Samples are selected at random for each training iteration.

**Table 4.5** Comparison of percentage of correct classifications by MLP and GMLC.

Theme	MLP	GMLC
Sugar Gums	73.33	85.78
Aleppo Pines	93.42	88.82
Open Fields	64.84	69.28
Lawns	99.38	99.38
Dirt Roads	98.47	98.47
Dull Metallic Roof	50.00	77.08
Specular Metallic roof	97.39	87.58
Bright Metallic Roof	90.00	96.67
Asbestos Roof	83.33	97.44
Dark Bitumen	75.23	100.00
Light Bitumen	74.16	78.52
Concrete	52.17	84.78
AVERAGE	79.31	88.65

Table 4.4 shows the confusion matrix for MLP classification using the same training areas as previous experiments and. Table 4.5 shows the relative accuracy of MLP and GMLC using the same training areas. The MLP has not been able to better the accuracy of GMLC in this test. Confusion is of the same kind as GMLC with Gums being misclassified as Pines, barren soil classified as open field and light bitumen being classified as dark bitumen. Other more troubling confusions occur between concrete and metallic reflectors. This is caused mostly by a very strong reflection from these

---

surfaces. Asbestos is also a problem, with some open fields being confused with Asbestos rooves. A major contributor to the good average performance in the GMLC case is the 100% accuracy for dark bitumen, for which the MLP only gets 75% correct.

Because the MLP can handle an arbitrary number of inputs, it is possible to reconfigure it to use texture in the training areas. In this demonstration of classification that was impractical because the training areas were selected for GMLC and as such were chosen not to have texture where possible, and many training areas were too small to make an estimate of texture. The potential for the use of the MLP in this way is discussed further in the reference by Whitbread (1992).

#### 4.8 Conclusions

This section has described a number of pattern recognition aids for interpreting satellite images and has shown how classification can be used to extract man-made objects. The standard GMLC has performed better than MLP in this study.

## 5 OBJECT HEIGHT DETERMINATION

In the last two decades enormous gains have been made in processing satellite images. However, the analyses of the images have remained mostly qualitative in nature, compared to the field of photogrammetry. This chapter presents an application of remote sensing for height determination using SPOT images.

Photogrammetrists have been able to extract the heights of objects from aerial photographs using parallax in stereo-pair photographs. The lengths of the shadows cast by the objects are also used to determine the heights. If the sun and sensor geometry is known it is fairly simple to establish a relationship between the shadow width and the height of the objects. The above usages, however, are confined to high resolution photographs or images.

### 5.1 Shadow - an important part of images

Shadows form a unique part of any image. They are easily detectable as they show a low intensity in all the multispectral bands. Shadows play a dominant role in image statistics which affect image enhancement and pattern recognition. Shadows contain 3-D information of objects and they have been used in object identification, terrain classification and geological mapping (Curran,1985).

Detection of objects by their shadow structures has been performed by many workers in the photogrammetric community (Venkateswar and Chellappa,1990; Irvin and McKeown,1989; Huertas and Nevatia,1988). All have utilised the nature of shadows around buildings to interpret the structure of the building. An edge detection routine has been used by Huertas and Nevatia (1988) that looks for different types of shadows that represent the corners of buildings in the aerial photographs. One of the problems Huertas and Nevatia (1988) encountered in their study was in identifying the shadows. Their technique failed to identify some areas of shadow or included areas that were not in fact shadow. Venkateswar and Chellappa(1990) have used knowledge based procedures to overcome some of these problems.

Although photogrammetrists have successfully used shadows in aerial photographs for height determination and object identification, the use of satellite images for similar purposes is not seen in the literature. The main reason is that the resolution of the civilian satellite images is much coarser than the aerial photographs and the shadows are not fully defined for short and commonly occurring objects.

### 5.2 Sun - satellite geometry and the equations

Figure 5.1 shows the sun-satellite geometry as an end view (2-D display of 3-D geometry for simplicity) for the two SPOT images used in this study. As illustrated in the figure the shadow part seen by the sensor is different for the two images. The width of the shadow, measured along the normal to the object, depends on the azimuths of the sun, image scan line and the object. The objects are rows of trees in this study (Figure 5.2).

In principle the procedure that is presented in this section is suitable for any object that casts detectable shadows of sufficient length. In the study area rows of trees cast shadows that could be used. Buildings were either not tall enough or long enough to cast a consistent shadow. For this reason the shadow detection and height analysis were initially performed on rows of trees. After establishing the relationship between the shadow widths and the measured heights, the heights of the unknown objects (buildings) were determined.

For relating shadow width to the object (tree) height a few basic assumptions were made. Firstly, the object is assumed to be vertical, that is the object is perpendicular to the earth's surface. Secondly, the shadows are assumed to be cast from the top of the object and that the top of the object is also the last part of the object seen from the sensor before the shadow begins. This assumption is not entirely satisfactory because there could be parts of object, between the illuminated part of the object and the ground shadow, not illuminated by the sun but seen by the sensor due to the scattered light. The computation assumes that the parts of the object not directly illuminated by the sun as part of the shadow. Thirdly, it is also assumed that the shadow starts from the tree-trunk line on the ground. Fourthly, as shown in Figure 5.1, it is assumed that if the sensor and the sun are on opposite sides of the object, then the sensor is able to see the entire shadow. Lastly, the surface that the shadow falls on is even and level.

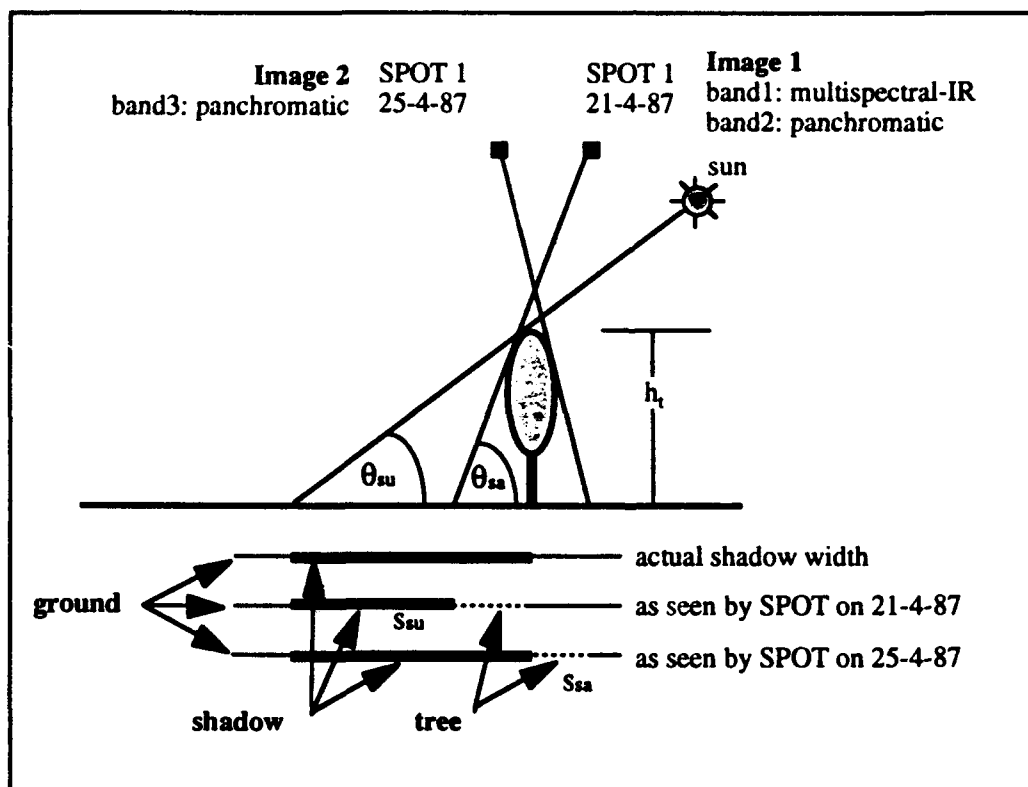


Figure 5.1 End view of the sun-satellite configuration as seen during imaging

The shadow width along the sun azimuth (Figure 5.1) is given by

$$s_{su} = h_t / \tan(\theta_{su}) \quad \dots\dots\dots (5.1)$$

The shadow width obstructed, along the azimuth of the sensor (Figure 5.1), by the object (tree) in the sensor's field of view

$$s_{sa} = h_t / \tan(\theta_{sa}) \quad \dots\dots\dots (5.2)$$

Shadow of the object along the normal to the tree line (Figure 5.2)

$$s_{sun} = s_{su} \cdot \cos(\phi_{sun}) \quad \dots\dots\dots (5.3)$$

Shadow obstructed by the object along the normal to the tree line (Figure 5.1)

$$s_{san} = s_{sa} \cdot \cos(\phi_{san}) \quad \dots\dots\dots (5.4)$$

where  $\phi_{sun} = \phi_{su} + 90 - \phi_t \quad \dots\dots\dots (5.5)$

and  $\phi_{san} = \phi_{sa} + 90 - \phi_t \quad \dots\dots\dots (5.6)$

The shadow width that is seen by the satellite is given by

$$s = s_{sun} - s_{san} \quad \dots\dots\dots (5.7)$$

Note that  $s_{san} = 0$  if the satellite is on the opposite side of object from the sun.

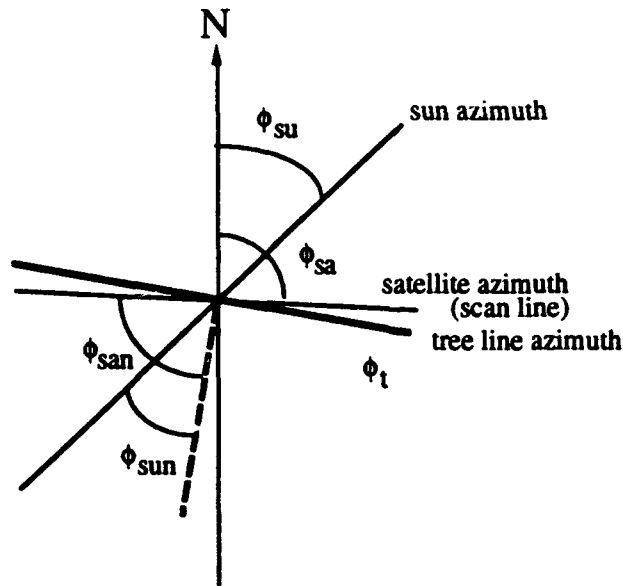


Figure 5.2 Plan view of the sun-satellite configuration as seen during imaging

For the panchromatic and multispectral image of 21st April 1987 the data are as follows:

$$\begin{aligned} \theta_{sa} &= 23.4^\circ \text{ and } \theta_{su} = 55.5^\circ \\ \phi_{sun} &= 13.2^\circ \text{ and } \phi_{san} = 76.5^\circ \dots\dots\dots \end{aligned} \quad (5.8)$$

Using equations (5.1) to (5.4) and (5.8) we get

$$h_t = 0.76 \text{ s} \quad \dots\dots\dots \quad (5.9)$$

If the tree or shadow line is at an angle to the image scan line, an additional correction needs to be applied to equation 5.9. This is because of the pixelisation of shadow zones. The issue is explained in Appendix II. The shadow width in equation 5.9 needs to be divided by  $\cos(\phi_{scan})$ , where  $\phi_{scan}$  is the angle between the scan lines and the tree line. For the rows of trees considered  $\phi_{scan} = 15^\circ$ . The relation used in this study is:

$$\begin{aligned} h_t &= 0.76 \text{ s} / \cos(\phi_{scan}) = 0.79 \text{ s} \\ &= k \text{ s} \quad \dots\dots\dots \end{aligned} \quad (5.10)$$

where k is a constant for objects of fixed azimuth in an image.

**5.3 Relationship between shadow width, pixel size and intensities**

The above relationships assume that the shadow zones are sharply defined and the pixel size is infinitesimally small. However, in practice neither the shadow zones are well defined nor the pixel sizes are negligibly small in relation to shadow widths. The following discussion presents simple relationship between pixel intensities and shadow boundaries.

If the brightness of the shadow (object) is  $I_0$  and that of the background is  $I_b$ , then the brightness of a pixel may be approximated to:

$$I_f = f I_0 + (1-f)I_b \quad \dots\dots\dots \quad (5.11)$$

where p is the area fraction of shadow in the pixel.

If  $I_0$  and  $I_b$  are known from pure shadow and background pixels, then

$$f = (I_f - I_b) / (I_0 - I_b) \quad \dots\dots\dots \quad (5.12)$$

There will normally be a threshold  $f_{min}$  such that if  $f > f_{min}$  then the pixel is classed as shadow. If not it is classed as background. Clearly, the representation of shadow in the image depends on the threshold chosen.

**5.3.1 The role of pixel dimension**

As we are considering the shadows cast by linear objects of length much greater than that of the pixel dimension, we will not lose any generality if we consider the

relationships only along a profile, say X axis, orthogonal to the object. If the shadow of length  $s$  of uniform intensity is centred at the origin of the profile and the pixel size  $p$  is smaller than the shadow size the intensity of pixels along the profile for various  $x$  is given by

$$f = \begin{cases} 0 & \text{for } x \leq \frac{-(s+p)}{2} & \text{(pixel outside object)} \\ \frac{(x+(s+p)/2)}{p} & \text{for } \frac{-(s+p)}{2} < x \leq \frac{-(s-p)}{2} & \text{(pixel partially on the object)} \\ 1 & \text{for } \frac{-(s-p)}{2} < x \leq \frac{(s-p)}{2} & \text{(pixel wholly within the object)} \\ \frac{(-x+(s+p)/2)}{p} & \text{for } \frac{(s-p)}{2} < x \leq \frac{(s+p)}{2} & \text{(pixel partially on the object)} \\ 0 & \text{for } x \geq \frac{(s+p)}{2} & \text{(pixel outside object)} \end{cases} \dots\dots\dots (5.13)$$

If the threshold is  $f_{min}$  then the estimated width  $w$  of the shadow of width  $s$  will be

$$w(p, f_{min}) = s + p(1 - 2f_{min}) \dots\dots\dots (5.14)$$

or in terms of estimated tree heights  $h_{est}$  and actual tree heights  $h_t$ , using relation equation 5.10

$$h_{est} = h_t + kp(1 - 2f_{min}) \dots\dots\dots (5.15)$$

which is a linear relationship between  $h_{est}$  and  $h_t$  with an intercept  $kp(1 - 2f_{min})$  and a slope 1. If  $f_{min}$  is very small, the intercept is roughly  $kp$  and if  $f_{min}$  is very high (near one), the intercept is roughly  $-kp$ . The intercept is zero for  $f_{min} = 1/2$ , which means that the boundary between the shadow and the background is half way between their respective intensities. In that case the estimated height is equal to the actual height. This relation assumes that  $p < s$ , object and background intensities are uniform, and that the measurement errors are normally distributed. In actual practice the latter two assumptions may not be true. As such, the above equations may only be used as a guide to arrive at an optimal  $f_{min}$ , through experiments, such that the intercept and the slope of the regression line in equation 5.15 are close one and zero respectively.

## 5.4 Shadow Segmentation

### 5.4.1 Choosing the threshold for delineating shadow zones

In high resolution images one might find a separate peak in the histogram corresponding to shadow areas, as described by Otsu (1979). In such cases it is easy to separate the shadow zones. In lower resolution images it is not common to find a separate peak for the shadow areas. The current study required a general procedure for

delineating shadows falling on various types of backgrounds. The backgrounds included lush grass, barren soil, white concrete and black asphalt covers. Experiments were conducted by choosing various thresholds by varying  $\alpha$  in the equation

$$f_{\min} = \mu - \alpha\sigma \dots\dots\dots (5.16)$$

where  $\mu$  and  $\sigma$  are mean and standard deviation of the image. Note that as  $\alpha$  increases the threshold decreases. The weight  $\alpha$  was varied from 1.6 to 0.8 in steps of 0.1. These two limits were found adequate as at a threshold of  $1.6\sigma$  most of the shadow areas were mis-classified as non-shadow areas and when a threshold of  $0.8\sigma$  is used most of the non-shadow areas were classified as shadow areas.

#### 5.4.2 Measurement of shadow width

From the accuracy point of view it would be better if the shadow width could be determined from SPOT panchromatic bands which have a resolution of 10 m. However, in panchromatic bands both the trees and shadows appear equally dark and the separation of the trees and shadows is not possible. However, in the infrared band of the multispectral image (Figure 5.3), which has a resolution of 20 m., the trees show a significantly higher reflectance than the surroundings and the shadow zones. In principle only the infrared band would suffice to determine the shadow width, but with a lesser precision due to its coarser resolution. In order to improve the accuracy of the estimate of the shadow width it was decided to use the panchromatic and infrared bands together. Another reason for using the combination is for shadow detection accuracy. A low value in infrared band does not necessarily mean that it is a shadow zone. For example bitumen surface gives a low reading in infrared, but a relatively higher value in panchromatic images. A combination of panchromatic and infrared bands would detect shadow zones better.

The image data consisted of an infrared band of a SPOT multispectral image and two panchromatic bands taken on two different days, as shown in Figure 5.1. The three bands were co-registered to form a 3-band image using control points at the ground level. Initially, for a chosen threshold,  $f_{\min}$ , shadow areas that were common to all the three bands were delineated. Using the same  $f_{\min}$  shadow areas common to only the infrared band and the panchromatic band of image 1 (Figure 5.1) were determined. No significant difference was found between the shadow zones determined in the two experiments. For this reason only the two bands of image 1 (Figure 5.1) were used for further investigation.

Figure 5.4 shows an example of the shadow segments delineated from the images. Using the segmented shadow areas an average shadow width is measured for each row of trees. As can be seen from Figure 5.4, the edges of the shadow areas are not straight. This is because of the alignment of the rows of trees at an angle to the scan lines and also due to the coarse pixel resolution. Due to the jagged nature of the shadow boundaries the estimation of the width is complicated. The average width was

---

estimated by measuring the area covered by each shadow zone and then dividing it by the length of the zone.

In order to accomplish the above procedures the shadow zones were vectorised using the program RASVEC<sup>®</sup> available on the Intergraph workstation. The areas bound by the polygons corresponding to the shadow areas were calculated using the MicroStation CAD software. Shadows of length less than 50 m were neglected. From the shadow width estimates of the tree heights were computed using equation 5.10.

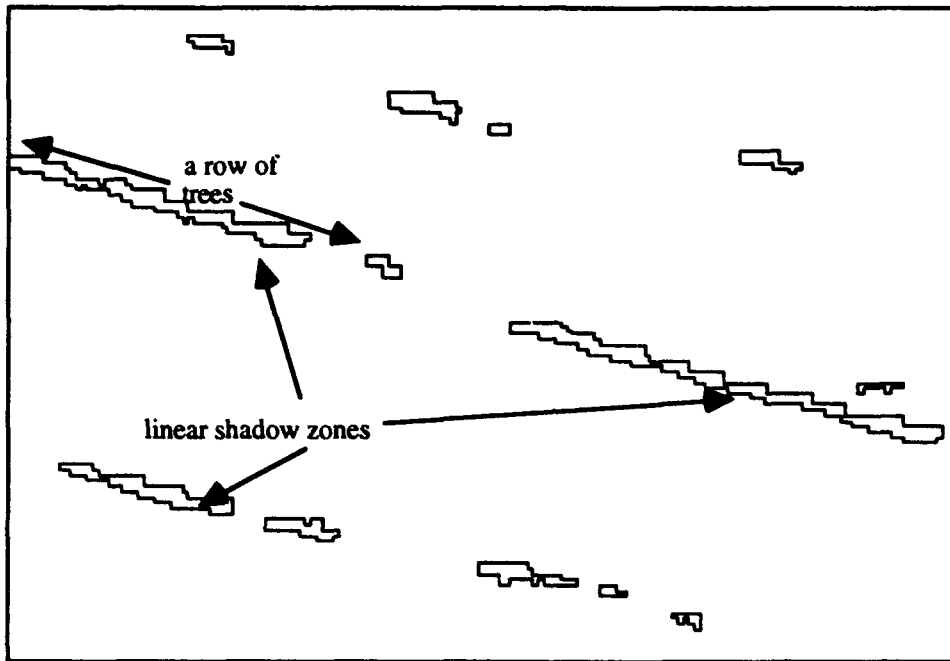




Figure 5.3 Infrared SPOT image of the study area. The rows of trees used in the study are marked and the buildings whose heights are estimated using the tree shadows are shown at the lower right hand corner.

## 5.5 Result and discussion

Most of the shadow zones shown in Figure 5.4 are correctly identifiable as cast by the rows of trees. However, false identification of shadow areas has also occurred. The dark bitumen at the west of the image and some wet market garden areas in the south western part of the image (Figure 5.3) were mis-classified as shadows. In this study no automatic procedures have been developed to isolate 'false shadow' zones.



**Figure 5.4** Shadow zones, shown as polygons, delineated using the thresholding procedure on the infrared and the panchromatic bands

There are some rows of trees that are parallel to the principal plane of the sun or the sun azimuth which do not cast shadow. No height estimation could be made for rows of trees with such an orientation.

Eight sites were selected for tree height estimation. At these eight sites tree heights were also measured. Table 5.1 summarises the measured tree heights and the estimated heights from the shadows.

Table 5.1 Estimated and actual tree heights

site no.	Shadow length m	Estimated tree height m	Measured average tree height m	Standard deviation of measurement m
2	29.720	21.82	17.90	1.41
1	27.635	20.28	17.45	2.34
3	35.390	25.98	15.00	1.37
4	29.705	21.81	17.96	1.35
5	25.191	18.50	15.82	1.11
7	11.119	8.25	11.76	0.64
6	28.323	20.80	16.14	1.26
8	25.359	21.55	17.11	0.63

Figure 5.5 shows the regression lines of estimated heights computed from shadow widths determined by using different thresholds and actual tree heights are shown. For the sake of clarity, regression lines and data points for only a few thresholds are plotted.

Notice that the correlation between the observed heights and the estimated heights deteriorate drastically when the threshold is increased from  $1.2\sigma$  to  $1.1\sigma$ . The variation of height estimates are shown for all the sites with these two thresholds. The height estimates increase systematically, as expected, for all the sites except site 5. The increase in height estimate for site 5 is disproportionately high. This is due to the inclusion of non-shadow areas in the shadow estimates. Notice that the regression line for any of the cases involving thresholds up to  $1.1\sigma$  do not pass through the origin as ideally we would have liked to. To achieve an intercept of zero the threshold has to be varied between  $0.9\sigma$  and  $0.8\sigma$ . However, as we increase the threshold above  $1.2\sigma$  background areas are increasingly classed as shadow areas. Thus the increase of threshold beyond  $1.2\sigma$  is not justifiable.

The coefficient of determination ( $r^2$ ) for thresholds higher than  $1.2\sigma$  is high (Figure 5.5). This indicates that the shadow estimates are very well correlated (correlation coefficient of 0.832 for threshold  $1.2\sigma$ ) to the measured tree heights. One point worth considering is that whether the number of points used for the regression is large enough. The probability of getting a correlation of above 0.8 is less than 6% when the two variables are uncorrelated, and the number of measurements involved is more than 6 (Taylor, 1982). This suggests the results of regression are reliable.

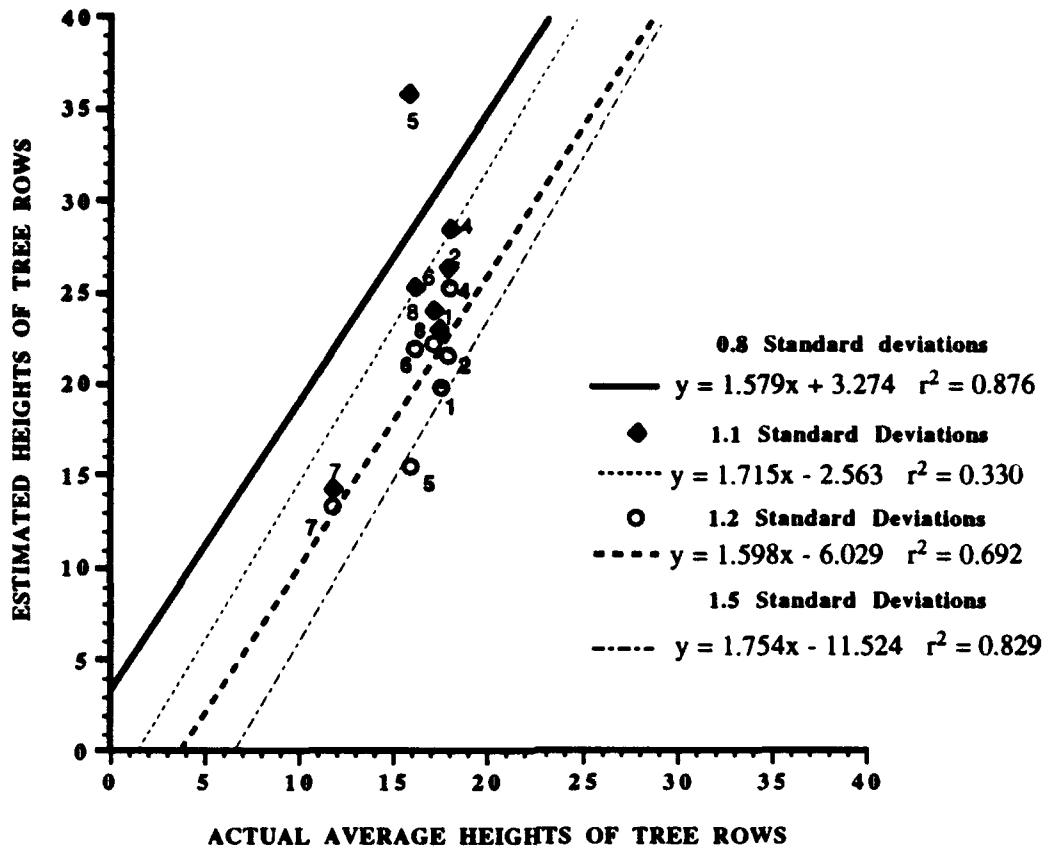
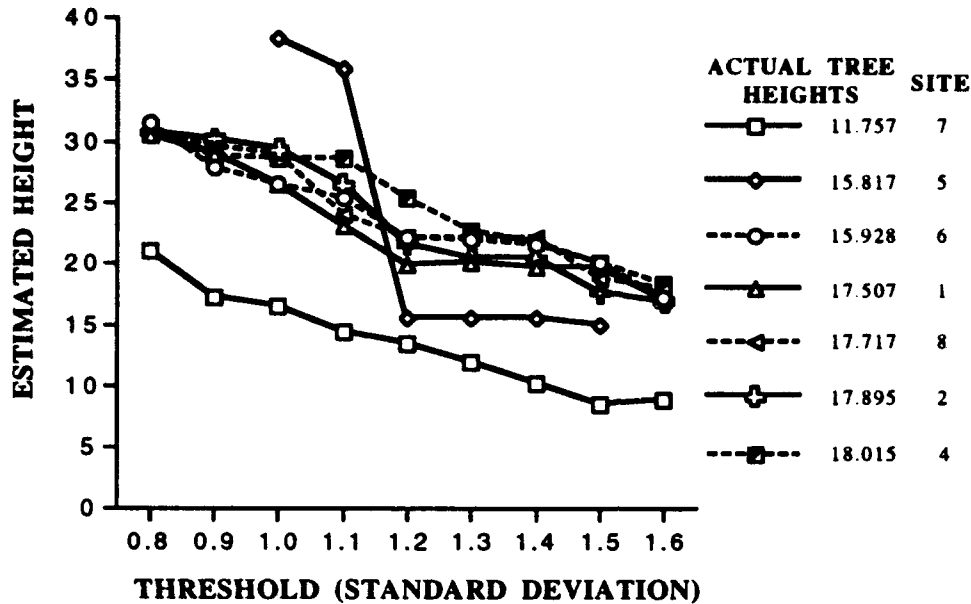


Figure 5.5 Regression lines for different thresholds. Notice that the estimated heights vary systematically for all the sites except for site 5. The drastic variation for site 5 is attributed to the inclusion of background areas when the threshold is increased from 1.2 to 1.1 $\sigma$ .

Figure 5.6 shows how estimated heights vary with various thresholds. Each line in the plot corresponds to a row of trees and a location. The plot reveals that all the estimates vary sharply between 1.2 $\sigma$  and 1.1 $\sigma$ , indicating that non-shadow areas are getting incorporated in the shadow estimates. This point is vividly illustrated by the site 5 estimate. As explained above the estimate for site 5 jumps drastically between 1.2 and 1.1 $\sigma$ . This indicates that the optimum threshold for separating shadows from the background exists between 1.2 $\sigma$  to 1.1 $\sigma$ .

It is also interesting to note that as the threshold is increased or decreased from 1.2 $\sigma$  the height estimates tend to be asymptotic. As such, the estimates for rows of trees within a range of heights tend to converge to a common value. These properties are currently being investigated using theoretical models. However, some heuristic explanation for this property may be given here.

In Figure 5.7 intensity curves are sketched for shadow zones of sharp boundaries and varying widths. The curves mimic the smoothing of sharp boundaries due to the point spread functions of the sensors. As can be seen, at A and B the intensity curves tend to overlap and at O they show maximum separation. Considering the noise inherent in images it may be expected that the closely spaced intensity curves can be inseparable at thresholds A and B. This explains the convergence of estimated tree heights at two extreme thresholds.



**Figure 5.6** Variation of estimated tree height with threshold. Notice that the estimated heights converge at two extreme thresholds. Also the gradient variation is maximum between 1.2 and 1.1 $\sigma$

Figure 5.8 is a three dimensional (3-D) display of the tree heights interpreted from the shadows in the image. The heights of the rows of trees has been vertically exaggerated by a factor of two. The 3-D display provides additional information apart from highlighting the tree heights. The gaps between the rows of trees get exaggerated, which otherwise may go unnoticed. For example, the rows of trees on the extreme left hand side of the image show a gap which is not evident in the 2-D display in Figure 3.2. The other rows of trees also give the impression of having numerous gaps. However, those could be artefacts created by the pixelisation of shadows.

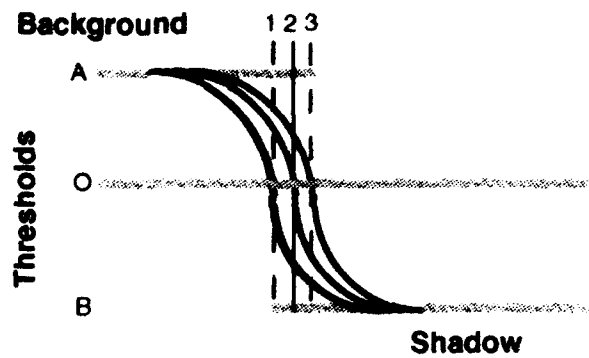


Figure 5.7 A sketch of intensity variation across shadow boundaries to demonstrate the variation of separability at various thresholds. The vertical lines 1, 2 and 3 represent the three sharp boundaries between shadow and background. The three curved lines represent the intensity variation as seen by the sensor across the three boundaries. The lines A, B and O represent the three thresholds and their thickness represents the possible noise level. At thresholds A and B the separation of the three curved lines is difficult to achieve, particularly considering the noise. At threshold O the curves stand separated.

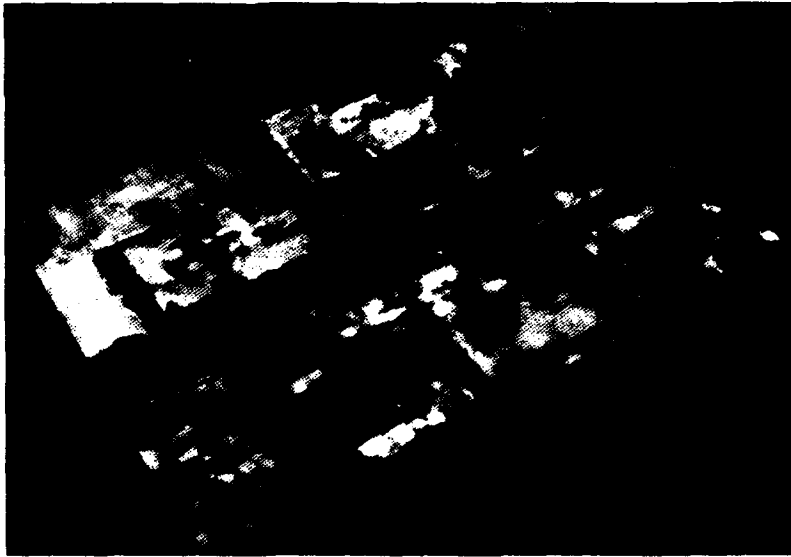


Figure 5.8 A three dimensional display of some rows of trees in the DSTO area.

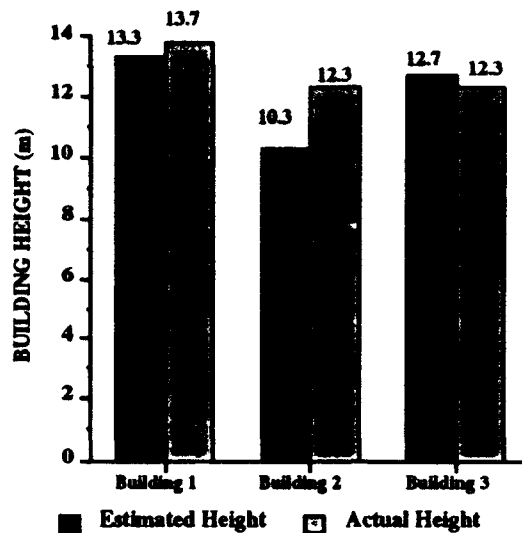


Figure 5.9 The plot of estimated and actual building heights of some industrial buildings

Based on the above analysis the regression line corresponding to  $1.2\sigma$  was taken as the optimum calibration line (Figure 5.5) to relate the estimated height from equation 5.10 to the actual height. Using the widths of shadows cast by the industrial buildings in the south-east of the image (Figure 5.3) the apparent heights were estimated using relation (equation 5.10). The actual heights were then estimated using the calibration line of Figure 5.5. The result is shown in Figure 5.9. As can be seen the estimated height closely follows the actual heights. A high sub-pixel accuracy of the order of one third of the pixel size has been achieved in this experiment.

### 5.6 Some limitations of the technique

The technique is useful for estimating heights of extended objects. The technique can not be used if the object does not cast a shadow, for example when the extended side of the object is parallel to the principal plane of the sun.

Area 3 (Figure 5.3) was not used in this study as it was found out early in the investigation that the shadow width delineated by the process was exceptionally large compared to the height of the trees. At site 3 two rows of trees were found. It is possible that the row of trees casting the first shadow is itself mostly hidden by the second row of trees. This will suppress the infrared reflectance from the first row of trees and the two shadow zones will appear as one as cast by the second row of trees. Due to the coarseness of the images it is difficult to ascertain the actual situation. However, it is important to eliminate such samples from the regression analysis.

It must be also realised that the data used in this study have been of a limited height range due to the rows of trees available in the area. A large range of heights would have been more suitable for the study.

## 6 NEW IMAGE ENHANCEMENT TOOLS

Many of the decisions by defence agencies or resource industries are done by visual pattern recognition as opposed to the numerical techniques explained in section 5. Image enhancement plays a major role in improving the visual pattern recognition in the images (Woodruff and Newsam, 1992). The background discriminant analysis technique described in section 4 is a tool in which objects of interest are enhanced in a multispectral image by suppressing the contribution of background information. In this section 2 other issues in image enhancement are addressed.

### 6.1 Smooth image zooming

The commercial satellite images have coarser resolution compared to aerial photographs which are conventionally used in defence for pattern recognition purposes. While displaying such images the objects look blocky making the recognition of the objects difficult. The problem becomes more severe as the observer zooms into a small area. While no extra information can be created in the blocky image once it is created, one can improve the presentation of the image to assist the human observer in understanding the image. Image smoothing while zooming (Woodruff and Newsam, 1992) is one way to reduce the blocking. In his approach, Newsam (1992) used a smooth interpolant to sub-sample an image to higher apparent resolution. An approximation is then determined to the interpolant using FFTs.

Using a similar approach as that of Newsam (1992), in this study cubic convolution is used for interpolation while zooming. Cubic convolution is a process originally developed for Landsat image reconstruction. Cubic convolution is simply another interpolation technique implemented by convolving the image samples with a smooth, spatially limited one-parameter functions constructed by joining cubic polynomials in a spline like fashion. It is generally accepted that this interpolation process gives a good compromise between complexity of computation and accuracy (Billingsley, 1983). The technique is generally superior to the standard image restoration procedures and it can be adapted to the frequency content of the image (Park and Schowengerdt, 1983).

In the field of remote sensing the cubic convolution interpolation is extensively used for resampling. The procedure is generally available in commercial software for registering images of two different pixel resolutions. Due to the increased processing speed and the possibility of subsampling the images in the main memory in near real time exists in most machines.

An existing command line procedure in ISI-2 image processing software on an Intergraph workstation was adopted for smooth zooming. The existing utility 'image to image' in ISI-2 can be used to subsample an image using cubic convolution procedure. The input parameters for the utility include the displayed image name, the name of the output (smooth zoomed) image to be displayed, and a file containing a table of ground control points. In the normal

application of the utility the ground control points are selected manually by comparing the image to be resampled and the reference image. In the current work the table of ground control points was generated automatically based on the zoom required. Table 6.1 demonstrates how the table is generated. The whole sequence of generating the ground control points table and smooth zooming of the image can be implemented as a command procedure and assigned to a function key. Depending on the size of the image and the processor speed the display can be in near real time.

**Table 6.1** Ground control points for zooming by a factor X

GCP location	Input Image line	Input Image pixel	Zoomed Image line	Zoomed Image pixel
top left corner	1	1	1	1
top right corner	1	n	1	nX
bottom left corner	m	1	mX	1
bottom right corner	m	n	mX	nX

Figure 6.1 is for demonstrating how an image may be zoomed in to achieve a magnification of 8. Figure 6.1(a) shows a sub-image of the GMH industrial complex adjoining the DSTO area. The image is shown at its full resolution of 10 m. Figure 6.1 (b) is the same image degraded to 80 m resolution, which is equivalent to a compression factor of 64. Each pixel in Figure 6.1 (b) is a mean of a 8x8 window. Figure 6.1 (c) is the smooth zoomed image derived from Figure 6.1(b) using cubic convolution. In Figure 6.1 (d) smooth zooming is achieved by the procedure of Newsam (1992). As can be seen the reconstructed Figures 6.1 (c) and (d) closely resemble the original full resolution image of 10 m. resolution in Figure 6.1 (a).

At this stage the results of smooth zooming from the two techniques have not been compared in any quantitative sense. The purpose of this example is simply to demonstrate the use of an existing remote sensing tool for a fairly complicated mathematical operation. The results from the two techniques are comparable.

Figure 6.2 is similar to Figure 6.1. The magnification in this case is 16 which is equivalent to 256 fold data compression. Clearly, the smooth zooming has not restored the image in Figure 6.2 (b) to the quality of Figure 6.2 (a). The zoomed images in Figures 6.2(c) and (d) also suffer from the distracting contouring effect. The contouring effect can be reduced to some extent, if desired, by dithering (Jain,1989).

From the above two examples it may be recommended that up to 8 times magnification can be achieved using smooth zooming without significantly degrading the image. Near real time

smooth zooming, using cubic convolution, can be implemented on most remote sensing image processing systems using vendor provided utilities.

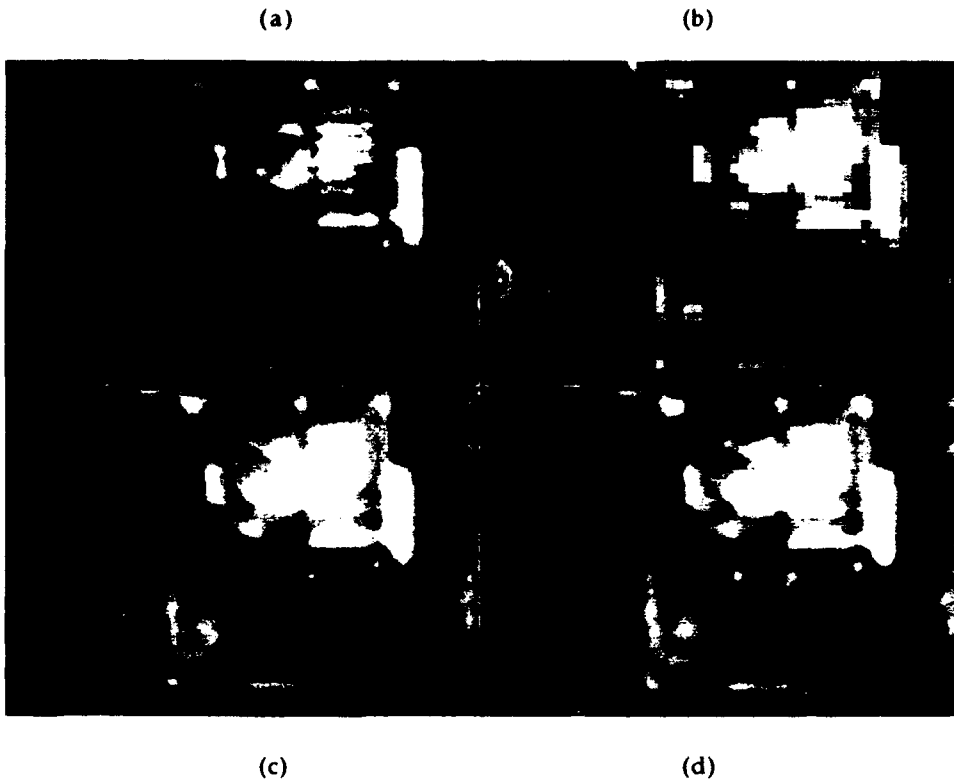
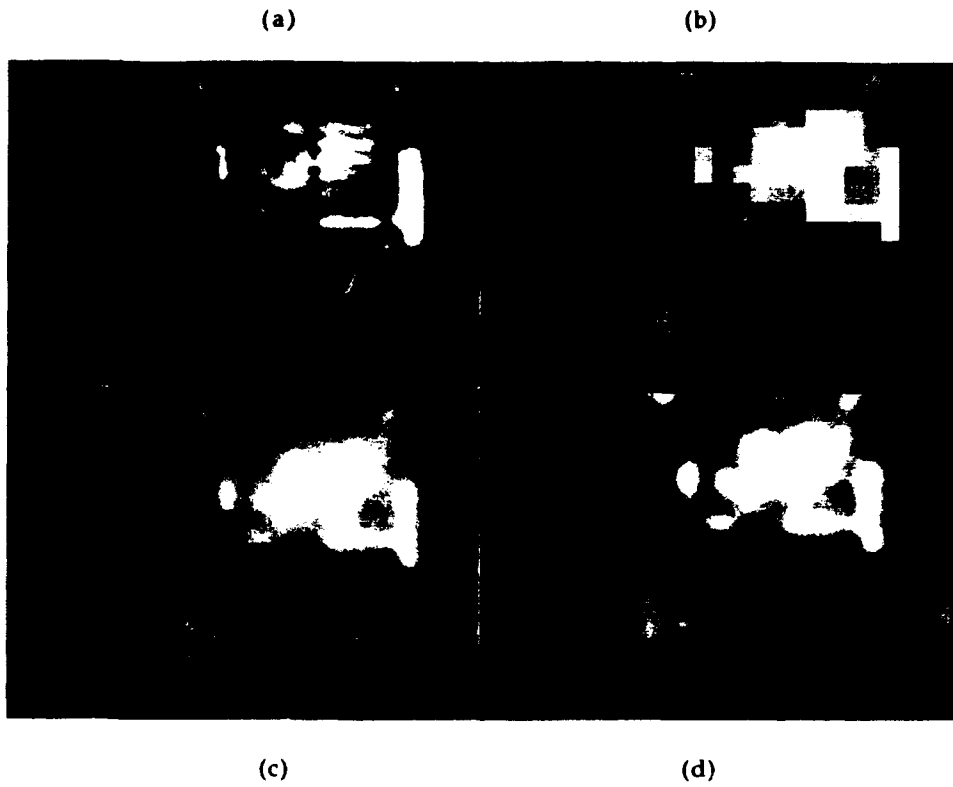


Figure 6.1 Smooth zooming by a factor of 4.

- (a) the original image of 10 m resolution
- (b) degraded image with 40 m resolution
- (c) image in (b) is smooth zoomed by a factor 4 using cubic convolution,
- (d) image in (b) smooth zoomed by a factor 4 using the interpolation technique of Newsam(1992)



**Figure 6.2** Smooth zooming by a factor of 8.

- (a) the original image of 10 m resolution
- (b) degraded image with 80 m resolution
- (c) image in (b) is smooth zoomed by a factor 8 using cubic convolution,
- (d) image in (b) smooth zoomed by a factor 8 using the interpolation technique of Newsam(1992)

---

## 6.2 Multispectral image enhancement by merging higher resolution panchromatic data

The availability of high resolution data in the form of panchromatic image data or scanned aerial photograph has given rise to a host of procedures to enhance coarser resolution multispectral images. By merging, the advantage of having both spectral and spatial resolution is gained. This will enhance the target recognition task. Shettigara (1992) has shown that the merging process can be achieved in one simple step of linear transformation. Due to this simplification it is possible to achieve merging of data in near real time and enhance the image on the screen at the location of interest.

To demonstrate the power of merging, the multispectral SPOT image of air base (figure 6.3.a) was merged with the panchromatic image taken at the same time (figure 6.3.b). As can be seen, merging has enhanced the parked aircraft on the apron, which is not clearly visible in the original multispectral image.

The merging was achieved in 3 steps:

1. the total intensity component of (a) was computed,
2. the total intensity component was substituted by the panchromatic data and,
3. the higher resolution information content in the new intensity component is re-distributed to the multispectral bands. The resultant image is shown in Figure 6.3(b).

Data merging can be achieved in many other ways. For more details the reader may refer to Shettigara (1992).

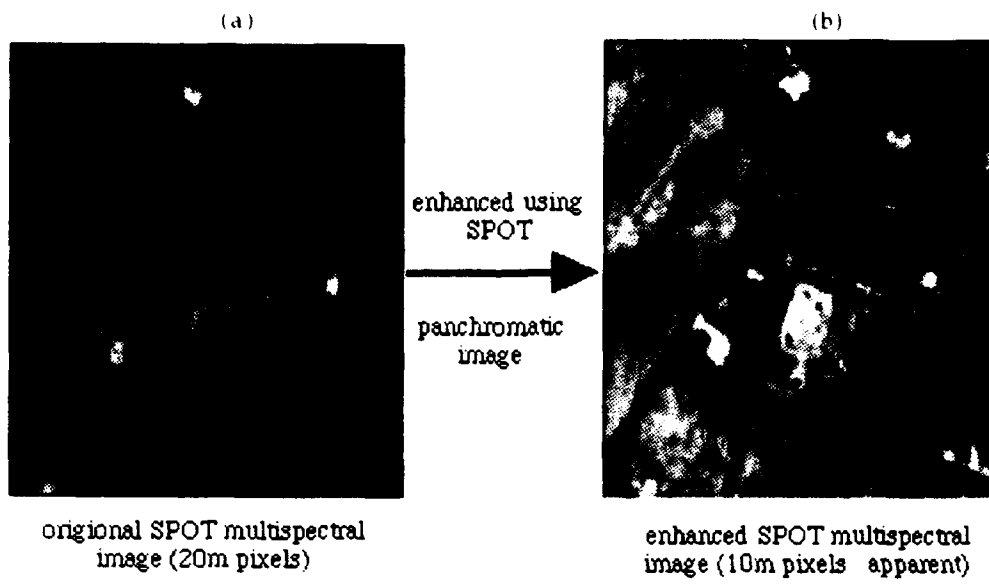


Figure 6.3 Merging of panchromatic image with the SPOT multispectral image

- (a) multispectral image
- (b) enhanced image by merging panchromatic image
- (c) Notice the 4 aircraft, below the circular compass swing, near the top right hand corner, enhanced in image (b) above

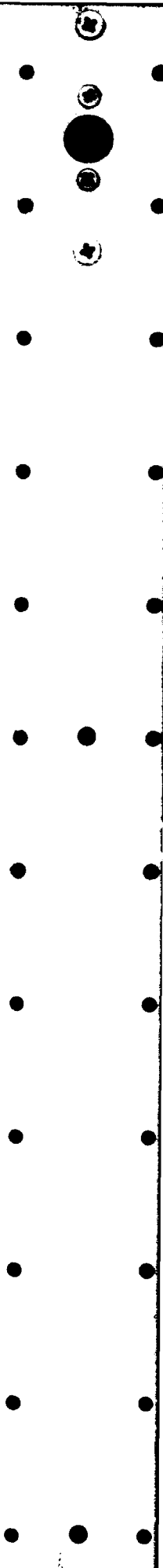
---

## 7 CONCLUSIONS

Some new capabilities of commercial satellite images have been demonstrated in this report. A particular effort has been made to use the images for quantitative purposes.

- ◆ It is shown that heights of extended targets can be determined to sub-pixel accuracy (2 to 3 m in our case) using SPOT multispectral and panchromatic images of 20 and 10 m pixels respectively. The high accuracy is achieved by developing a procedure for optimal segmentation of the shadows. The same procedure may be extended to determine other dimensions of the targets, such as the widths of roads or the lengths of buildings.
- ◆ The conventional statistical pattern recognition techniques and neural net approaches are used for object classification. An accuracy of the order of 87 % achieved in classifying artificial objects.
- ◆ New techniques are demonstrated for image resolution enhancement in computer displays. It is shown that an image whose resolution is degraded by a magnitude of up to 8 can be smooth zoomed, using cubic convolution resampling, to achieve a look similar to the original. Smooth zooming can be of great assistance in target detection.

The report clearly demonstrates the ability of multispectral satellite images in enhancing and detecting targets of defence significance. Objects such as aircraft can be clearly detected and different types of buildings can be discriminated. It is also possible to determine heights or other dimensions of targets, larger than the pixel size, to sub-pixel accuracy. As mentioned in the introduction, the applications of commercial satellite images are very much dependent on the data analysing expertise. In view of this there is a need to re-assess the capabilities of civilian satellite images in surveillance and intelligence gathering.



---

**BIBLIOGRAPHY**

- Avery T. E., 1969 *Interpretation of Aerial Photographs*, Burges Publishing Company, Minneapolis.
- Anderson, J.A., 1982, Logistic discrimination, in *Handbook of Statistics*, vol.2, p. 169-191 (P.R.Krishnaiah and L.K.Kanal eds., North Holland, Amsterdam).
- Anson P. and Cummings D., 1991, *The first space war - the contributions of satellites to the Gulf war*.
- Bernard, C., 1991, *SPOT: A key role in the Gulf war*, *Defence and Technologies International*, Dec. 1991.
- Benediktsson, J. A., Swain, P.H., and Esroy, O.K., 1990. Neural Network Approaches Versus Statistical Methods in Classification of Multi-Source Remote Sensing Data. *IEEE Transactions on Geoscience and Remote Sensing* 28(4): 540-552.
- Billingsley, F.C., 1983, Data processing and reprocessing, in *Manual of Remote Sensing* Ch17, 2nd ed., p719-792.
- Crist E.P. and Cicone, R.C., 1984, A physically based transformation of thematic mapper data - the TM tasseled cap, *IEEE Trans. Geoscience and Rem. Sensing*, GE22, p256-263.
- Curran, P.J., 1985, *Principles of remote sensing*, Longman Scientific & Technical, Essex, 282p.
- EOM (*Earth Observation Magazine*), 1992, November issue, p10.
- Gale, W., 1992, The potential of satellite for wide area surveillance of Australia, *Fellowship paper*, Royal Australian Airforce, Air Power Studies Centre. 158p
- Goward, S., N. and Wharton, S. W., 1984. Use of the TM tasseled cap transform for interpretation of spectral contrasts in an urban scene, *1984 Machine Processing of Remotely Sensed Data Symposium*, pp. 84 - 91
- Heermann, P. D. and Khazenie, N., 1992. Classification of Multispectral Remote Sensing Data Using a Back-Propagation Neural Network." *IEEE Transactions Geoscience and Remote Sensing* 30(1): 81-88.
- Hepner, G. F., T. Logan, Ritter, N, and Bryant, N., 1990. Artificial Neural Network Classification Using a Minimal Training Set: Comparison to Conventional Supervised Classification. *Photogrammetric Engineering and Remote Sensing* 56(4): 469-473.
- Huertas A. and Nevatia R., 1988 Detecting Buildings in Aerial Images, *Computer Vision, Graphics, and Image Processing*, Vol. 41, pp 131-152.
- Hyland, S., Lennon, P. and Luck, P. 1988. An assessment of Landsat Thematic Mapper to monitor seagrass in Moreton Bay, southern Queensland. *Symposium on Remote Sensing of the Coastal Zone, Queensland, 1988*, pp. VA. 4.1.- VA. 4.15.
- Iisaka, J. and Russell, W., 1991, Using Neural networks in remote sensing image processing, *Proceedings IGARSS'91, Helsinki*, p2223.
- Ioka, M., and Koda, M. 1986. Performance of Landsat-TM data in land cover classification. *International Journal of Remote Sensing*, 7(12), pp .1715-28.
- Irvin B. R. and McKeown D. M., 1989 Methods for Exploiting the Relationship Between Buildings and Their Shadows in Aerial Imagery, *IEEE Transactions on Systems, Man and Cybernetics*, Vol. SMC-19 No. 6, pp 1564-1575.

- 
- Joye,A.M.R.,1991, Satellite surveillance over the north, *FDA draft working paper*, SURV 4, 71p.
- Jain,A.K., 1989, *Fundamentals of digital image processing*, Prentice Hall Inc.,NY,569p.
- Kanellopoulous, I., Varfis,A., Wilkinson, G.G. and Megier, J., 1991. Classification of Remotely Sensed Satellite Images Using Multi-Layer Perceptron Networks. *Artificial Neural Networks*. Elsevier Science Publishers. 1067-1070.
- Klemas, V., Bartlett, D., and Rogers. 1975. Coastal zone classification from satellite imagery. *Photogrammetric Engineering and Remote Sensing*, 41(4), pp. 499-513.
- Lachenbruch, P.A. and Goldstein,M.,1979, Discriminant Analysis, *Biometrics*,35,69-85.
- Mundy,J.L.,1991, Model-based vision, an operational reality ?, *SPIE*,1567,p124-141.
- McKeown, D.M.Jr, 1990, *Built-up area feature extraction: second year technical progress report*, ETL-0562
- Newsam,G.N., 1992, Smooth zooming in images (submitted for publication)
- Otsu N., 1979 A Threshold Selection Technique from Gray-level Histograms, *IEEE Transactions on Systems, Man and Cybernetics*, Vol. SMC-9 No. 1, pp 62-66.
- Park S.K. and Schowengerdt R.A.,1983, Image reconstruction by parametric cubic convolution, *Computer vision,Graphics, and Image Processing*,23,258-272.
- Richards,J.A.,1986, *Remote Sensing Digital Image Analysis - An introduction*, Springer-Verlag,Berlin,281p.
- Richelson J.T.,1990,Implications for nations without space-based intelligence-collection capabilities, in *Commercial observation satellites and international security* , St Martin press NY. Ed: Krepon, M., Zimmerman P.D., Spector L.S. and Umberger M., pp55-73.
- Rumelhart, D. E., Hinton, G.E., and Williams, R.J., 1986. Learning Internal Representations by Back Propagation Errors. *Nature* 323(0): 533-536.
- Sali, W. and Wolfson, H. 1991 Texture classification in aerial photographs and satellite data. *Artificial Intelligence and Computer Vision*, Elsevier Science Publishers B. V., North-Holland, pp 325-34
- Sheldon, R. A., 1990. Satellite Image Analysis using Neural Networks. *Telematics and Informatics* 7(3/4): 431-439.
- Shettigara,V.K.,1991, Image enhancement using background discriminant transformation, *Int J. Remote Sensing*,12,p.2153-2167.
- Shettigara,V.K.,1991a, Robustness of Gaussian maximum likelihood and linear discriminant classifiers, *Proceedings IGARSS91,Helsinki*,p1839-42.
- Shettigara,V.K.,1992, A generalised component substitution technique for spatial enhancement of multispectral images using a higher resolution data set, *Photogrammetric Engineering and Remote Sensing*,58,pp 561-567.
- Sleigh,A.C.,1983, *Image understanding for military systems: a discussion of the way forward for PRIP research in Britain*, Memorandum 3560. (PRIP stands for pattern recognition and image processing.)
- Swain, P. H., and Davis, S. M., 1978, *Remote Sensing: The Quantative Approach*, McGraw - Hill, New York.
- Taylor,J.R.,1982, An introduction to error analysis, *University science books*,Oxford university press,Mill Valley,270p.
-

- 
- Thomas, I.L., Ching, N.P., Benning, V.M. and D'Aguanno, J.A., 1987, A review of multi-channel indices of class-sparability, *Int.J.Remote Sensing*, 8, p. 331-350.
- Venkataswar V. and Challappa R., 1990, A Framework for Interpretation of Aerial Images, *IEEE*, pp 204-206
- Wharton, S. W. (1987). A spectral knowledge based approach for urban land cover discrimination. *IEEE Transactions on Geoscience and Remote Sensing*, 25(3), pp. 272 - 82
- Wheeler, D. J. (1986) Spectral characterization of urban land covers for Thematic Mapper data, *Symposium on Remote Sensing for Resources Development an Environmental Management*, pp 893 - 98
- Whitbread, P. J., 1992. *Multi-spectral Texture: Improving Classification of Multi-spectral Images by the Integration of Spatial Information*. PhD Thesis, University of Adelaide, South Australia.
- Woodruff C.J. and Newsam G.N., 1992, Displaying undersampled images, (submitted for publication)
- Young T.Y. and Calvert T.W., 1974, *Classification, estimation and pattern recognition*, Elsevier, NY, 366p.
- Zimmerman P.D., 1990, Introduction (to photo-interpretation of commercial observation-satellite imagery), in *Commercial observation satellites and international security*, St Martin press NY. Ed: Krepon, M., Zimmerman P.D., Spector L.S. and Umberger M. pp201-204.



## APPENDIX I

TABLE I.1 GROUND RESOLUTION REQUIREMENTS FOR INTERPRETATION OF IMAGERY

Target <sup>a</sup>	Detection <sup>b</sup>	General ID <sup>c</sup>	Precise ID <sup>d</sup>	Description <sup>e</sup>	Tech analysis <sup>f</sup>
Bridges	6	4.5	1.5	1	0.3
Communications					
Radar	3	1	0.3	0.15	0.015
Radio	3	1.5	0.3	0.15	0.015
Supply dumps	1.5-3	0.6	0.3	0.03	0.03
Troop units (in bivouac or on road)	6	2	1.2	0.3	0.15
Airfield facilities	6	4.5	3	0.3	0.15
Rockets and artillery	1	0.6	0.15	0.05	0.045
Aircraft	4.5	1.5	1	0.15	0.045
Command and Control HQ	3	1.5	1	0.15	0.09
Missile sites (SSM/SAM)	3	1.5	0.6	0.3	0.045
Nuclear weapons components	2.5	1.5	0.3	0.03	0.015
Vehicles		0.6	0.3	0.06	0.045
Surface ships	7.5-15	4.5	0.6	0.3	0.045
Land mines	3-9	6	1	0.03	0.09
Ports and harbours	30	15	6	3	0.3
Coasts, landing beaches	15-30	4.5	3	1.5	0.15
Railroad yards and shops	15-30	15	6	1.5	0.4
Roads	6-9	6	1.8	0.6	0.4
Urban areas	60	30	3	3	0.75
Terrain		90	4.5	1.5	0.75
Surfaced submarines	7.5-30	4.5-6	1.5	1	0.03

Notice that only the targets within the box have any possibility of detection using Landsat TM or SPOT images. Only very large targets can be identified in general.

- <sup>a</sup> Chart indicates minimum resolution in meters at which target can be detected, identified, described, or analysed. No source specifies which definition of resolution (pixel-size or white-dot) is used, but the chart is internally consistent.
- <sup>b</sup> Detection: location of a class of units, object, or activity of military unit.
- <sup>c</sup> General identification: determination of general target type.
- <sup>d</sup> Precise identification: discrimination within target type of known types.
- <sup>e</sup> Description: size/dimension, configuration/layout, component construction, equipment count, etc.
- <sup>f</sup> Technical analysis: detailed analysis of specific equipment.

Adapted from Richelson, 1990

**TABLE I.2 TARGET DETECTION CAPABILITIES OF COMMERCIAL SATELLITE IMAGES**

Target <sup>a</sup>	Detection <sup>b</sup>	General Identification <sup>c</sup>	Quantitative <sup>d</sup>
Bridges	MSS/TM	TM/XS	XS/P
Roads	MSS	MSS	TM/XS
Radars	P	P	
Railroads	MSS	P	
Supply dumps	MSS	P	P
Major headquarters	MSS	TM/P	P
Airfield facilities	MSS	TM	P
Aircraft	P	P	P
Rockets and artillery	MSS/TM	XS/P	
Missile sites (SAM)	MSS	MSS/TM	P
Surface ships	XS	XS	XS/P
Surfaced submarines	TM(?)	XS/P	P(?)
Vehicles	P(?)		

Compare this table with Table I.1

Notice that the capabilities of the sensors are much more than earlier believed.

**Abbreviations:**

MSS: LANDSAT multi-spectral scanner; 80 meter resolution

TM: LANDSAT thematic mapper; 30 meter resolution

XS: SPOT extended spectrum sensor; 20 meter resolution

P: SPOT panchromatic sensor; 10 meter resolution

- <sup>a</sup> No attempt made to list all targets in original chart.
- <sup>b</sup> A target of the given type is clearly present, but no details are apparent.
- <sup>c</sup> Class of bridge, number of buildings, etc, can be discerned. There is little or no doubt that the target has been properly classified.
- <sup>d</sup> Quantitative measurements of the target can be made; aircraft classified as to mission or type. Known types can be recognised using tables, silhouettes, etc.

---

## APPENDIX II

### PIXELISATION EFFECT ON SHADOW WIDTH MEASUREMENT

In analytical terms the determination of width of a linear object can be achieved in many ways. One simple approach is to divide the area covered by the object by its length. This approach can not be directly implemented in image processing for computing shadow widths.

In Figure II.1 shadows are drawn as the area between pairs of lines. Widths are indicated opposite to the pairs of lines. The surface is divided into 10x10 m grids to simulate SPOT image pixels. The black pixels are those in which 50% or more of the pixel area is covered by shadow. It is assumed that a perfect technique is available to threshold such pixels and label them as shadows.

Due to the discrete pixel sizes involved in images the shadow zones may appear as continuous areas or as fragments. Under perfect thresholding conditions, as described above, one can expect continuous shadow zones only if the shadows have widths equal to or greater than the pixel dimensions.

From the figure it is also clear that the shadow width computed by dividing the area of shadow pixels by the length needs to be corrected. For example, the area covered by the 10 m. wide shadow is 20 pixels or 2000 m<sup>2</sup>. The length of the shadow is 208.8 m. The computed width of the shadow is 9.58, which is less than 10 m. In order to get the correct estimate the length must be measured along the scan line or the actual length must be multiplied by the cosine of the angle between the shadow zone and the scan line.

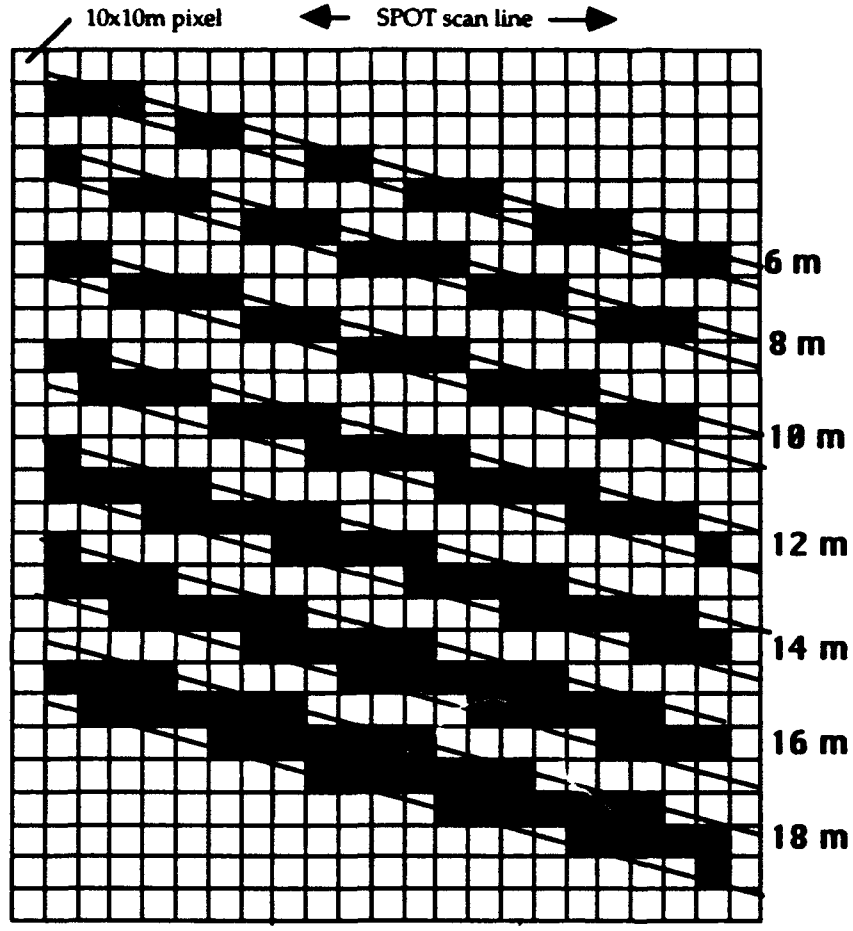


**Figure II.1** A sketch to show pixelisation effect on shadow detection and shadow width measurement. If shadow width is smaller than the pixel dimension the fragmentation of the shadow zone may be expected.

## DISTRIBUTION

	No of Copies
<b>Defence Science and Technology Organisation</b>	
Chief Defence Scientist )	
Central Office Executive )	1 shared copy
Counsellor, Defence Science, London	Cont Sht
Counsellor, Defence Science, Washington	Cont Sht
Scientific Adviser POLCOM	1
Senior Defence Scientific Adviser	1
Assistant Secretary Scientific Analysis	1
<b>HQADF</b>	
DGFD(L)	1
<b>DIO</b>	
Image Exploitation Centre	1
<b>Navy Office</b>	
Navy Scientific Adviser	1
<b>Air Office</b>	
Air Force Scientific Adviser	1
<b>Army Office</b>	
Scientific Adviser, Army	1
<b>Electronics Research Laboratory</b>	
Director	1
Chief, Information Technology Division	1
Chief, Communications Division	Cont Sht
Chief, Electronic Warfare Division	Cont Sht
Chief, Guided Weapons Division	Cont Sht
Research Leader, Command & Control and Intelligence Systems	1
Research Leader, Military Computing Systems	1
Research Leader, Human Computer Interaction	1
Head, Program and Executive Support	1
Head, Command Support Systems Group	1
Head, Intelligence Systems Group	1
Head, Information Management Group	1
Head, Systems Simulation and Assessment Group	1
Head, Exercise Analysis Group	1
Head, C3I Systems Engineering Group	1
Head, Software Engineering Group	1
Head, Trusted Computer Systems Group	1
Head, Computer Systems Architecture Group	1
Head, Information Acquisition & Processing Group	1
Mr V. K. Shettigara (Author)	1
Mr G. M. Sumerling (Author)	1
Mr P.J. Whitbread (Author)	1

---

Publications & Publicity Officer, ITD	1
<b>Surveillance Research Laboratory</b>	
Director	1
Chief, Land Space and Optoelectronics Division	1
<b>Libraries and Information Services</b>	
Australian Government Publishing Service	1
Defence Central Library, Technical Reports Centre	1
Manager, Document Exchange Centre, (for retention)	1
National Technical Information Service, United States	2
Defence Research Information Centre, United Kingdom	2
Director Scientific Information Services, Canada	1
Ministry of Defence, New Zealand	1
National Library of Australia	1
Defence Science and Technology Organisation Salisbury, Research Library	2
Library Defence Signals Directorate	1
British Library Document Supply Centre	1
<b>MHQ</b>	
MCAUST	1
<b>CSIRO Division of Water Resources</b>	
Dr D.L.B.Jupp	1
<b>USATEC</b>	
Dr M.B.Satterwhite	1
<b>Spares</b>	
Defence Science and Technology Organisation Salisbury, Research Library	6

---

**Department of Defence**  
**DOCUMENT CONTROL DATA SHEET**

1. Page Classification Unclassified
2. Privacy Marking/Caveat ( of document )

3a. AR Number AR-008-137	3b. Laboratory Number ERL-0694-RR	3c. Type of Report RESEARCH REPORT	4. Task Number	
5. Document Date NOVEMBER 1993	6. Cost Code	7. Security Classification	8. No. of Pages 76	9. No. of Refs. -
10. Title  SOME DEFENCE APPLICATIONS OF CIVILIAN REMOTE SENSING SATELLITE IMAGES		<input type="checkbox"/> U <input type="checkbox"/> U <input type="checkbox"/> U Document    Title    Abstract		
		S (Secret) C (Confl ) R (Rest) U (Unclass) * For UNCLASSIFIED docs with a secondary distribution LIMITATION, use (L) in document box.		
11. Author(s) Vittala K. Shettigara Gordon M. Sumerling and Paul J. Whitbread		12. Downgrading/Delimiting Instructions  N/A		
13a. Corporate Author and Address  Electronics Research Laboratory PO Box 1500, Salisbury SA 5108		14. Officer/Position responsible for  Security:.....N/A.....  Downgrading:....N/A.....  Approval for Release:...DERL.....		
13b. Task Sponsor				
15. Secondary Release Statement of this Document  APPROVED FOR PUBLIC RELEASE				
16a. Deliberate Announcement  No Limitation				
16b. Casual Announcement (for citation in other documents)  <input checked="" type="checkbox"/> No Limitation <input type="checkbox"/> Ref. by Author , Doc No. and date only.				
17. DEFTEST Descriptors  Remote sensing Satellite imagery Image analysis Military applications Military intelligence			18. DISCAT Subject Codes  080201	
19. Abstract  This report is on a pilot study to demonstrate some of the capabilities of remote sensing in intelligence gathering. A wide variety of issues, both quantitative and qualitative, are addressed. SPOT satellite images were used for object classification using statistical and neural net techniques, object height determination and image resolution enhancement. A new procedure was developed for detecting small and man-made objects in multispectral or colour images. The procedure will be presented in a companion report.				